NIST United States Department of Commerce
National Institute of Standards and Technology

NIST Technical Note 1493

Robot Crane Technology
(Final Report)

Nicholas G. Dagalakis, James S. Albus, Howard A. Bloomfield, Adam D. Lytle,
Tsai Hong, Tony L. Hopkins, Roger Bostelman, and Geraldine S. Cheok

The National Institute of Standards and Technology[1] was established by an act of Congress on March 3, 1901. The Institute's overall goal is to strengthen and advance the Nation's sciences and technology and facilitate their effective application for public benefit. To this end, the Institute conducts research to assure international competitiveness and leadership of U.S. industry, science and technology. NIST work involves development and transfer of measurements, standards and related science and technology, in support of continually improving U.S. productivity, product quality and reliability, innovation and underlying science and engineering. The Institute's technical work is performed by the National Measurement Laboratory, the National Engineering Laboratory, the National Computer Systems Laboratory, and the Institute for Materials Science and Engineering.

The National Measurement Laboratory

Provides the national system of physical and chemical measurement; coordinates the system with measurement systems of other nations and furnishes essential services leading to accurate and uniform physical and chemical measurement throughout the Nation's scientific community, industry, and commerce; provides advisory and research services to other Government agencies; conducts physical and chemical research; develops, produces, and distributes Standard Reference Materials; provides calibration services; and manages the National Standard Reference Data System. The Laboratory consists of the following centers:

- Basic Standards[2]
- Radiation Research
- Chemical Physics
- Analytical Chemistry

The National Engineering Laboratory

Provides technology and technical services to the public and private sectors to address national needs and to solve national problems; conducts research in engineering and applied sciences in support of these efforts; builds and maintains competence in the necessary disciplines required to carry out this research and technical service; develops engineering data and measurement capabilities; provides engineering measurement traceability services; develops test methods and proposes engineering standards and code changes; develops and proposes new engineering practices; and develops and improves mechanisms to transfer results of its research to the ultimate user. The Laboratory consists of the following centers:

- Computing and Applied Mathematics
- Electronics and Electrical Engineering[2]
- Manufacturing Engineering
- Building Technology
- Fire Research
- Chemical Engineering[3]

The National Computer Systems Laboratory

Conducts research and provides scientific and technical services to aid Federal agencies in the selection, acquisition, application, and use of computer technology to improve effectiveness and economy in Government operations in accordance with Public Law 89-306 (40 U.S.C. 759), relevant Executive Orders, and other directives; carries out this mission by managing the Federal Information Processing Standards Program, developing Federal ADP standards guidelines, and managing Federal participation in ADP voluntary standardization activities; provides scientific and technological advisory services and assistance to Federal agencies; and provides the technical foundation for computer-related policies of the Federal Government. The Laboratory consists of the following divisions:

- Information Systems Engineering
- Systems and Software Technology
- Computer Security
- Systems and Network Architecture
- Advanced Systems

The Institute for Materials Science and Engineering

Conducts research and provides measurements, data, standards, reference materials, quantitative understanding and other technical information fundamental to the processing, structure, properties and performance of materials; addresses the scientific basis for new advanced materials technologies; plans research around cross-cutting scientific themes such as nondestructive evaluation and phase diagram development; oversees Institute-wide technical programs in nuclear reactor radiation research and postdoctoral programs; and broadly disseminates generic technical information resulting from its programs. The Institute consists of the following divisions:

- Ceramics
- Fracture and Deformation[2]
- Polymers
- Metallurgy
- Reactor Radiation

---

[1] Headquarters and Laboratories at Gaithersburg, MD, unless otherwise noted; mailing address Gaithersburg, MD 20899.

[2] These divisions within the Institute are located at Boulder, CO 80303.

[3] Located at Boulder, CO, with some elements at Gaithersburg, MD.

NIST Technical Note 1267

Robot Crane Technology (Final Report)

Nicholas G. Dagalakis, James S. Albus, Kenneth R. Goodwin, James D. Lee,
Tsung-Ming Tsai, Hoosh Abrishamian, Roger Bastelman

Robot Systems Division
Center for Manufacturing Engineering

and Charles Yancey

Structures Division
Center for Building Technology

National Engineering Laboratory
National Institute of Standards and Technology
Gaithersburg, MD 20899

Sponsored by:
Defense Advanced Research Projects Agency (DARPA)
1400 Wilson Boulevard
Arlington, VA 22209-2308

July 1989

NOTE: As of 23 August 1988, the National Bureau of Standards (NBS) became the National Institute of Standards and Technology (NIST) when President Reagan signed into law the Omnibus Trade and Competitiveness Act.

U.S. Department of Commerce
Robert A. Mosbacher, Secretary

National Institute of Standards and Technology
Raymond G. Kammer, Acting Director

National Institute of Standards
and Technology
Technical Note 1267
Natl. Inst. Stand. Technol.
Tech. Note 1267
60 pages (July 1989)
CODEN: NTNOEF

U.S. Government Printing Office
Washington: 1989

For sale by the Superintendent
of Documents
U.S. Government Printing Office
Washington, DC 20402

TABLE OF CONTENTS

Robot Crane Technology

Executive Summary

The objective of the Robot Crane Technology Program is to develop kinematically constrained, dynamically stabilized, robot cranes capable of lifting, moving, and positioning heavy loads over large volumes, capable of supporting fabrication tools and the inspection of large size and difficult to reach structures.

Among the significant technologies pursued are:

* Achieve a better theoretical understanding of the properties of the proposed crane suspension mechanism, such as stiffness, dynamics, and stability.

* Demonstrate the use of the robot crane mechanism for factory automation, such as loading and unloading of machines, and moving heavy fixtures.

* Demonstrate the use of the robot crane mechanism for the fabrication and maintenance of large and difficult to reach structures, such as airplanes, ships, and submarines.

* Demonstrate the use of the robot crane mechanism for the accurate and efficient positioning of heavy payloads for the construction of airplanes, ships, submarines, buildings, dams, and bridges.

The approach taken builds on previous work at the NIST Robot Systems Division which has analyzed and measured the stiffness of a small model six-cable suspension system. This system is a modified Stewart platform.

Under DARPA sponsorship, we have;

1. Extended this work to measure and optimize the stiffness of full-size models.

2. Actively damped oscillations in a small scale six-cable suspension platform.

3. Constructed an intermediate sized six-cable suspension platform for an industrial robot.

Progress in the period from April 1 to November 31, 1988:

* A theoretical model of the proposed robot crane suspension mechanism has been developed and tested with a full-size robot crane model. The stiffness of the crane suspension mechanism for a full-size model was measured using two different types of external loads and compared with the theoretical model's predicted values. The full-size model suspension consisted of six wireropes of 3/8-in diameter, which supported a total load of approximately 19,000 lb, from a height of approximately 29 ft. The stiffness to a horizontal external force and the stiffness to a moment about the vertical axis applied to the lower suspended platform were measured. In the first case the theoretical model predicted stiffness averaged 14.6% less than that measured by the experiment. In the second case the theoretical model predicted stiffness averaged 33.8% less than that measured by the experiment. At the present, the wireropes have been replaced with new ones of 3/4-in diameter and a more thorough investigation of this difference is planned.

* The proposed crane suspension stiffness optimization problem was formulated. The optimization problem was studied for four different external loads. These were an external horizontal force, an external vertical force, a moment about the vertical axis, and a moment about a horizontal axis. Each of these loads was applied to the lower suspended platform. A global and a local maximum analysis study were conducted and general design rules were formulated. The selection of the maximum stiffness design depends on the type of external forces and moments which are expected to dominate the loading of the lower crane platform. The most convenient way to proceed with the selection of a design is probably to pick a few different sizes of the upper crane platform and then follow the rules described in section 4.2 for the selection of the lower platform size. The combination of the upper and lower platform with the highest stiffness is the best choice. The results of the optimization search have been tabulated and can be used to facilitate the design process.

* A three degree-of-freedom, robot crane, payload vibration compensation device was constructed and tested on a small crane model. This device consisted of a servo-driven horizontal X-Y table and rotary joint about the vertical axis, which was suspended from the model crane lower platform. The oscillations of the payload in the horizontal plane and its rotations about the vertical axis were detected by external sensors and a digital

controller determined the appropriate command signals to the servo-drives in order to compensate them. A simple proportional gain digital controller algorithm was used for this stage of the investigation. The gains were selected experimentally to minimize the number and amplitude of the oscillations of the payload in the corresponding direction. The payload response to force disturbances along the horizontal plane showed a significant improvement when the vibration compensation control was on. The payload response to moment disturbances about the vertical axis did not show any noticeable improvement when the vibration compensation control was on.

* An intermediate-size model robot crane was constructed for factory automation applications. Its upper platform was an equilateral triangle with a side length of 6 ft. Based on the stiffness optimization study, the lower platform was selected to be one-half the size of the upper platform. A PUMA-560[1] robot arm was suspended from the lower platform of this model. A robot tracking laser interferometer was used to monitor the movements of the arm in three-dimensional space and software was written to process and display the path tracking data. The robot arm turned out to be quite stiff to any type of external disturbances. Above a certain level, though, the wireropes would buckle, making the arm feel very soft [see fig. 12 of Dagalakis, N. G., et al., 1988]. This breakaway feature could be very desirable for applications where safety requires that the forces or moments applied by the robot arm do not exceed certain limits.

Proposed future work:

* Theoretical study and measurement of the buckling characteristics of the robot crane suspension mechanism.

* Design and test active damping and the micro-positioning control systems of an intermediate scale crane platform.

* Add vision, touch, and force sensors and demonstrate the ability of a robot crane to load and unload machine tools in a factory environment.

1 Products named in this report are listed for purposes of information only. There is no implied endoresement of any product or implication that they are the best available for the purpose.

* Develop the proper sensors and grippers and demonstrate the ability of a robot crane to pickup and deliver heavy fixtures in a factory environment.

* Develop the proper sensors and grippers and demonstrate the ability of a robot crane to provide lateral support to do drilling and deburring of large and inaccessible sheet metal structures.

* Retrofit a tower crane, develop the proper sensors and grippers and demonstrate the ability of a robot crane to pickup and deliver heavy payloads of different shapes and sizes for construction work.

Robot Crane Technology

1. Introduction

1.1 Objective

The objective of the Robot Crane Technology Program is to develop kinematically constrained, dynamically stabilized, robot cranes capable of lifting, moving, and positioning heavy loads over large volumes, capable of supporting fabrication tools and the inspection of large size difficult to reach structures.

1.2 Approach

Our approach built on previous work at the NIST Robot Systems Division to analyze and measure the stiffness of small model six-cable suspension systems. These systems are modified Stewart platforms.

Extend this work to measure and optimize the stiffness of full-size models, and actively damp oscillations in the six-cable suspension platforms.

Design and construct a six-cable suspension platform and control system for an industrial robot so the robot can move and work anywhere on or above a factory floor suspended by six cables from a bridge crane.

1.3 Background

The last 10 years have seen a tremendous growth in the use of robots in the manufacturing industry with more than 20,000 units installed in the United States, most of them in the automotive or automotive-related industries [U.S. Department of Commerce, 1987]. Amidst this astounding technological development, the application of robots in the large-scale fabrication, assembly and heavy construction industry is virtually nonexistent in the United States. The reasons for delay are because probably these are made-to-order industries, requiring precision in the construction of components and blocks, requiring an enormous number of structural members and machines most of which are heavy and bulky. In the case of heavy construction equipment, delays occur because they operate in a more complex and unconstrained environment - that of the construction site.

Airplane manufacturing and shipbuilding, which are heavy assembly and construction industries, being labor intensive, are becoming more expensive every year while robotic automation is becoming less expensive and more capable every year.

In Japan, the Japanese Shipbuilding Society started a 5-year research and development plan of "Modernization of Production Technology in Japan" in 1982 [Kubo, M., 1987]. The program is sponsored by a consortium of seven major Japanese shipbuilders, and funded by the Japan Foundation for Shipbuilding Advancement. As a result of this effort, prototypes of large size gantry-type robots for welding, surface preparation, and painting of ship structures have been built by Ishikawajima-Harima Heavy Industries Co. and are now being tested by Sumitomo Heavy Industries, Ltd.

Currently, ordinary cranes are stable only in the vertical direction. The load is free to rotate in all directions and sway in the horizontal plane under the slightest side pressure, similar to a pendulum. Under these conditions it would be very difficult for the crane to support any robotic operations due to the excessive compliance and low damping of its end-effector. Automatic crane antisway control devices have been proposed and tested by several people [Kogure, H. et al., 1978, Carbon, L., 1976, Gercke, U.S. Patent No. 2,916,162]. Although these devices tend to suppress the pendulum motions in the horizontal directions they fail to suppress any pitch, roll or yaw rotations of the load. Other systems have been developed which try to solve the sway problem by employing several wires and winches [Noly, U.S. Patent No. 4,350,254]. These systems add considerable complexity and cost to the load-handling system and have not found practical application thusfar.

Conventionally designed robots have been scaled up and used as cranes, but they are largely impractical for handling heavy loads. Due to the low payload-to-manipulator arm/weight ratio of these robots, they have to be constructed of gigantic dimensions, occupy a large floor area, and consume large amounts of power.

NIST has proposed a new crane design, which despite its simplicity, results in a very stiff load platform which can be used as a robot base or end-effector for heavy loads.

2. The Proposed Crane Suspension Mechanism

Considering the requirements for a robot crane, which should provide superior stiffness to load roll and sway, have a large work volume without occupying any significant floor space, and have a reasonable size, we have proposed the mechanism concept shown in figure 1 [Albus, J. S., 1987]. It consists of an equilateral triangular platform suspended by six wireropes, two at each vertex of the triangle, from an overhead carriage. The carriage can be attached to either an overhead (see fig. 2) or a boom crane, depending on the application. The carriage includes a single winch onto which all six wireropes attach as shown in figure 3, and rope guides which guide the six wireropes away from the winch in three pairs equidistantly spaced [Albus, J. S., et al., 1987]. If desired, it is possible to control the lengths of the individual wireropes with actuators or brakes properly positioned either at the lower platform or the carriage.

The suspended platform behaves as if it is supported by an extendable single solid beam with its elastic properties dependent on the weight of the load and the height of the crane for a given crane geometry and wirerope type and size. This is a significant improvement in stiffness over a conventional crane. It enables the load to be accurately positioned and provides a stable platform which can be used to exert torques and side forces on objects being positioned. The suspended platform can be used as a stabilized base for the direct mounting of conventional manipulator arms as shown in figure 2, or it can be used for the support of special substructures for specific crane applications. These robot crane designs can also be used for factory automation where they offer several advantages as compared with the usual current practice of having a manipulator dedicated to serve each machine tool. These advantages are higher payload and fewer manipulators, which hang from overhead rails and thus do not occupy valuable factory floor space.

The suspension mechanism of the proposed robot crane platform shown in figure 1 imitates the behavior of a parallel link manipulator arm. The arm mechanism is called parallel because the links are positioned side by side, "approximately" parallel to each other and each link serves a role "approximately" equal to that of its neighbor. This is different from the design of the more common serial link manipulators built of a chain of links connected end-to-end in a serial manner. Parallel link manipulators are, in general, known for the simplicity of their mechanical design, and their high strength and stiffness-to-weight ratios, because their actuators bear no moment loads but act in simple tension or compression. They are also known for their high force and moment capacity, since their actuators all act in parallel. Such manipulators with solid adjustable length beams in the place of the wireropes were first used for the design of tire test machines [Gough, V. E. et al., 1957, 1962]; later they were used for the design of flight simulators [Stewart, D., 1965].

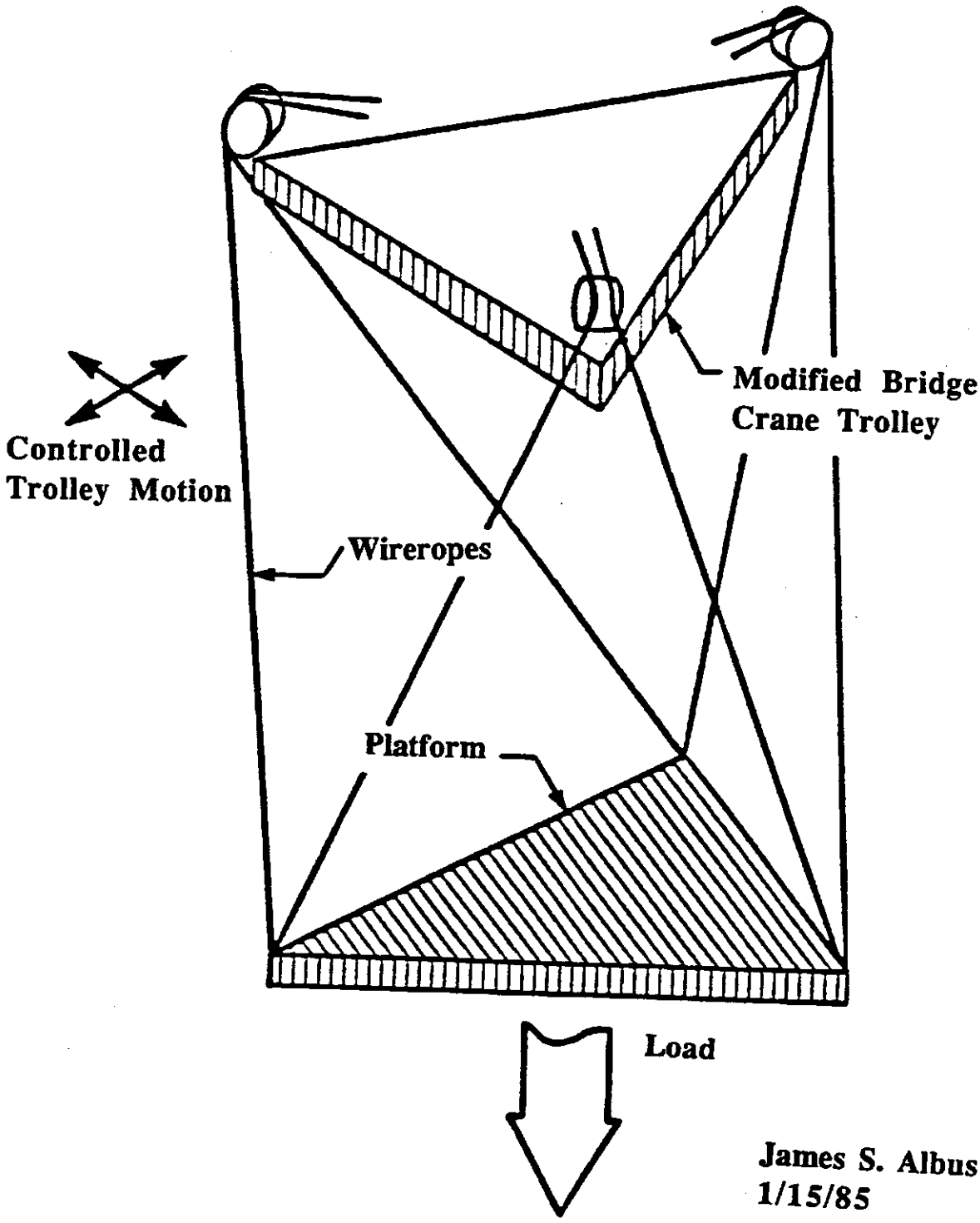

Figure 1. Mechanism concept.

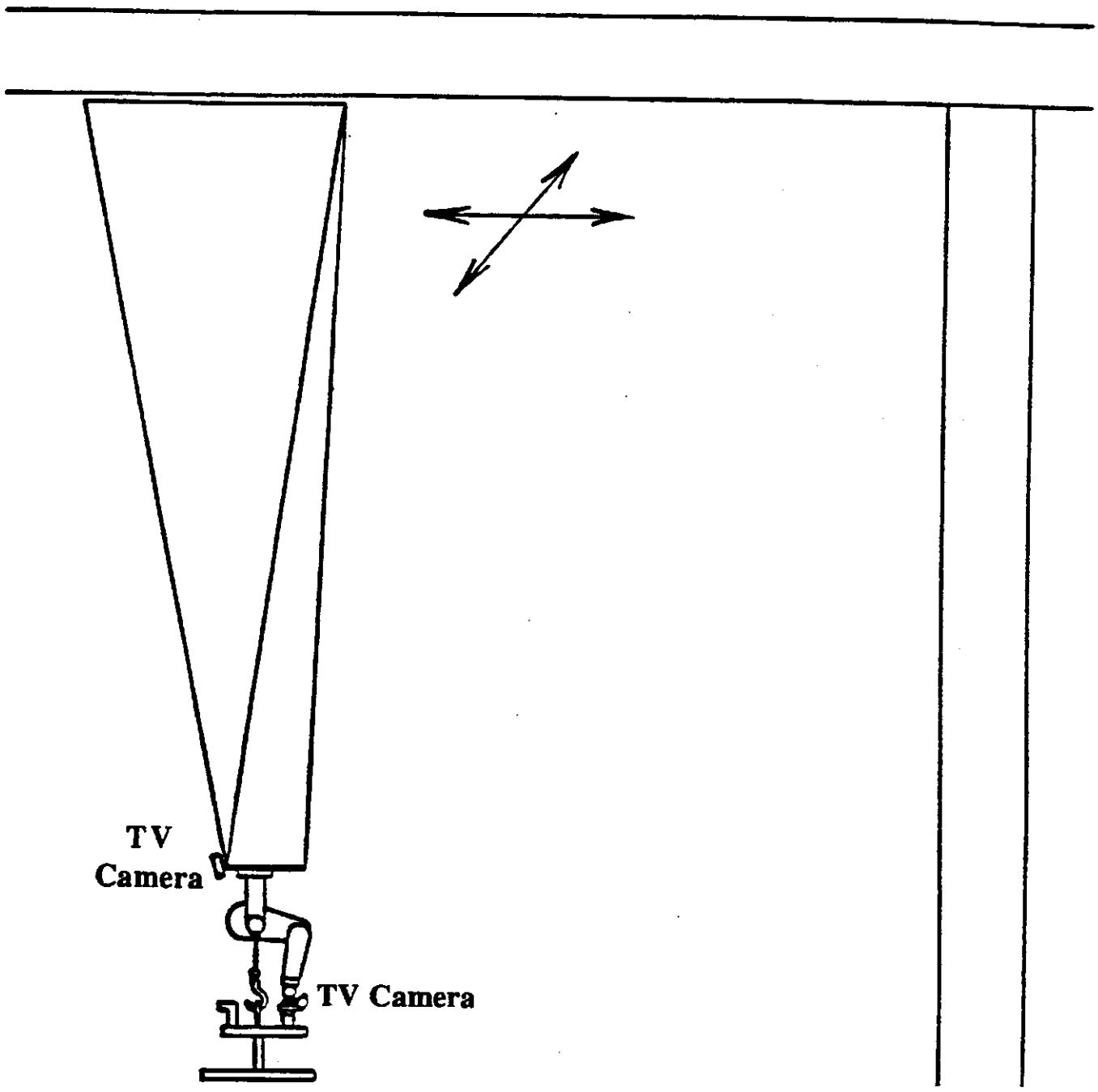

Figure 2. Overhead crane and robot manipulator combination.

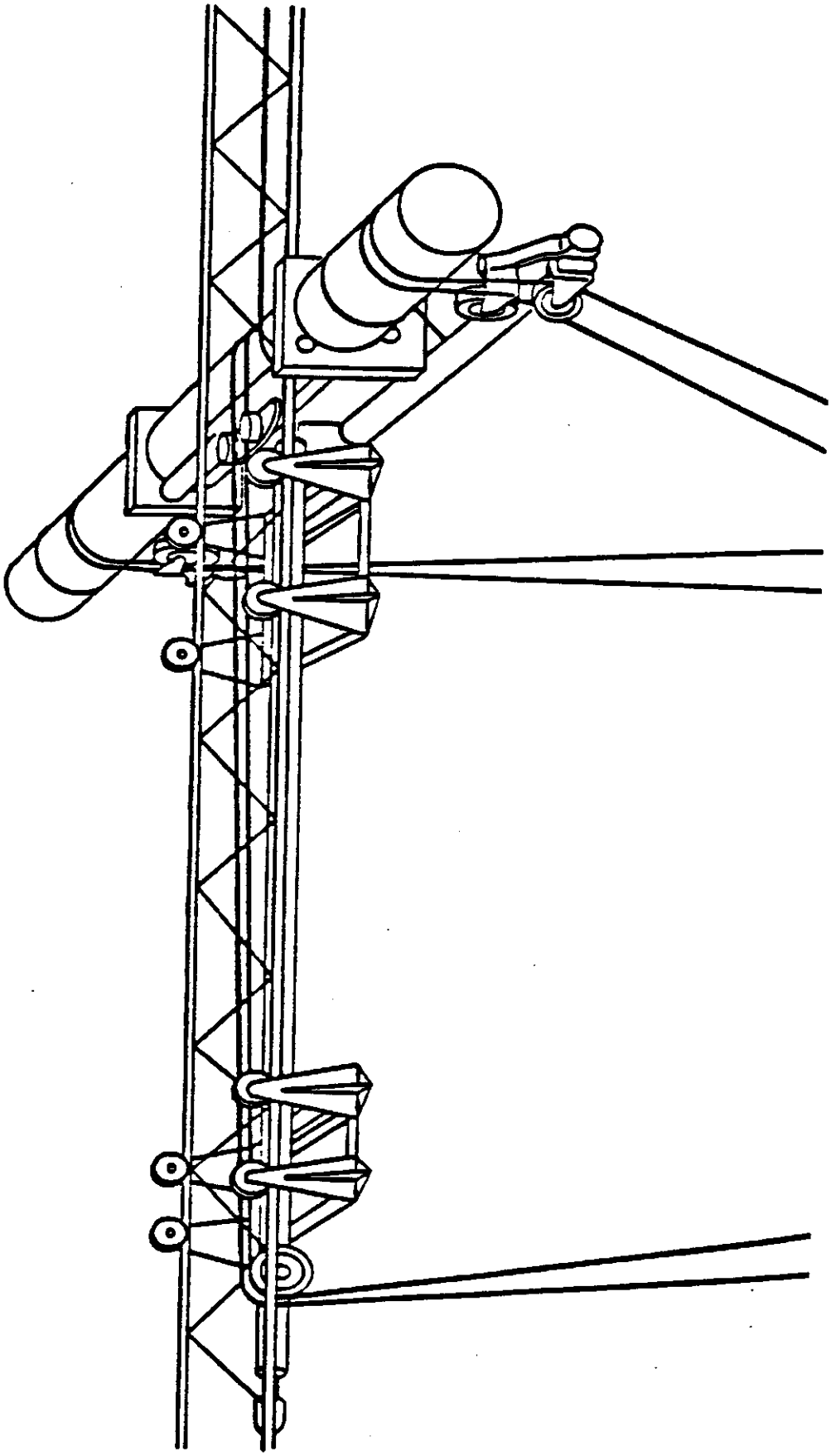

Figure 3. Cable suspension carriage with winch.

3. NIST Work Prior to April 1, 1988

A small model of the proposed robot crane suspension mechanism was constructed. The model consisted of two aluminum triangular plates of equal side length 228.6 mm (9.0 in), see figure 1. The lower platform was suspended by six steel wires. The height, which ranged from 3 to 4.5 ft, and the suspended weight W, which ranged from 100 to 350 lb, varied depending on the test conditions. During testing, external loads (force or moment) of various amplitudes and orientations were applied through a multiaxis load-cell. The resulting displacement in the direction of load application was measured.

A full-size model of the crane suspension mechanism with a lateral translation end-load outfitting subplatform structure, also was built, as shown in figure 4. It consists of a support frame mounted on the concrete reaction wall of a seismic test facility and two I beams connected at a 90 degree angle. These two beams are suspended by six wires from the support frame at approximately a 29-ft height and form the model of the lower platform and the subplatform structure. Each wire is connected to these beams through a load-cell for monitoring its tension and a turn-buckle for adjusting its length. The load, approximately 5,000 lb and the counter balance weight, approximately 10,000 lb, are simulated by lead bricks placed in two baskets which hang from the two ends of the long boom beam. This model was instrumented and used for the testing reported in this work.

A computer model of the proposed robot crane stiffness based on the nonlinear equations of the quasi-static motion of the lower platform was developed. Assuming small motions of the lower robot crane platform, a linearized equations model of the stiffness was developed. The small robot crane model test results were used to calculate the stiffness to external loads and to compare with the predicted values from the theoretical models. This work was described in [Dagalakis, N. G., et al., 1988].

With the increasing interest in robotic arm manipulators, studies have been conducted for their use as a mechanical wrist [Bennett, W. M., 1968], a compliant device [McCallion, H., at.al., 1979], a force/moment or position sensor [Koliskor, A. S., 1982], a robot arm [Fichter, E. F., et al., 1980, 1984, 1987, Powell, I. L., 1982, Landsberger, S. E., et al., 1985, Sheridan, T. B., 1986, Konstantinov, M. S., et al., 1985], and an industrial manipulator for assembly [Gadfly, 1983] and for grinding[Multicraft, 1987].

The design discussed here takes advantage of the suspended crane load to maintain the wireropes in tension and thus form six flexible wires which, with their elastic deformation, oppose any displacement of the payload. The stiffness created by this elastic deformation is superimposed onto the pendulum-effect-created-stiffness of ordinary cranes. Individual rope length control of the position and orientation of the platform is also possible.

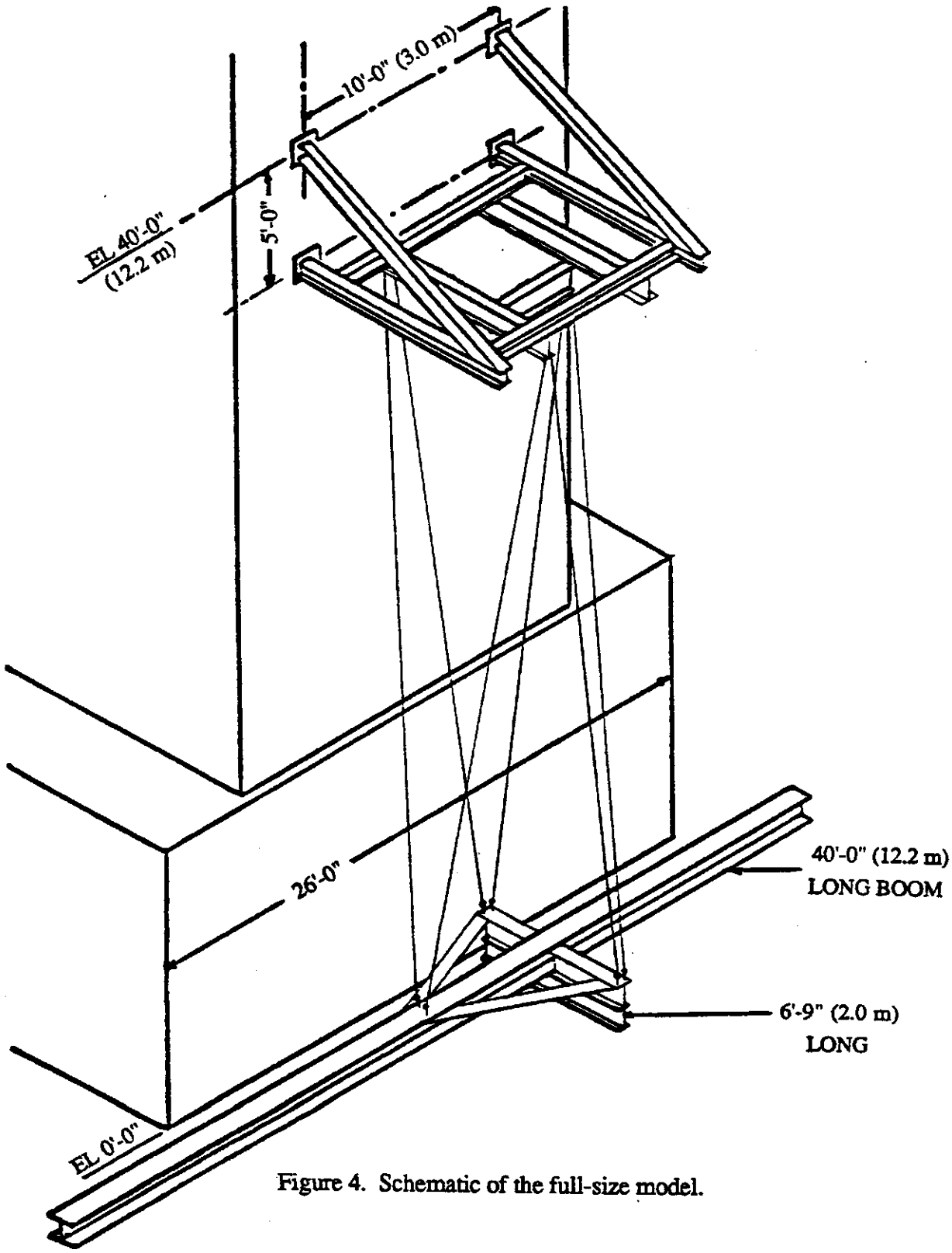

Figure 4. Schematic of the full-size model.

4. Report of the Progress in the Period From April 1 to November 31, 1988

4.1 Task I

The objective of this task was to measure the stiffness of a full-size model of the proposed robot crane suspension mechanism subjected to certain types of external loads and to compare the results with those predicted by the theoretical model. The theoretical model was previously developed and is described in [Dagalakis, N. G., et al., 1988].

A full-size model with a lateral translation end-load outfitting subplatform structure was completed and used for the experimental work required for this task. Figure 4 shows a schematic drawing of this model. The upper and lower platforms were constructed from steel I beams. The upper platform was mounted on a specially designed steel frame which was then attached to the side of a seismic reaction wall. The two platforms were constructed as equal equilateral triangles with a side length of 6 ft. The vertical distance between the platforms was 28.6 ft. The lower platform was suspended from the wireropes through six turn-buckles and six load-cells. The turn-buckles allowed compensation for small differences of the wirerope lengths and made possible the leveling of the lower platform. The load-cells were used to monitor the tensions of the wireropes. The length of four of the wireropes was 25.8 ft, while the length of the other two was 24.8 ft. The difference in lengths was due to the I beam construction of the upper platform. The total weight suspended from the lower platform was 19,100 lb.

Due to the large magnitude of the external load forces and moments involved special heavy fixtures had to be constructed to perform the stiffness measurement tests. A heavy optical bench was used for the application of horizontal side forces and two large stanchions for the application of pure moments. The translation and rotation of the lower platform was measured with a pair of displacement transducers.

The wireropes used to suspend the lower platform were 3/8-in diameter, 6x19 classification, with fiber core. In order to measure their Young's modulus of elasticity and stiffness it was decided to obtain their stress strain curve. Three small specimens, each 3-ft in length were prepared and tested on a materials testing machine. They were loaded and unloaded twice during each test. The stiffness of the wirerope at 3,000 lb tension force of the second loading cycle was used to calculate the modulus of elasticity. Its average value was found to be 13, 170, 208. lb/in^2.

The measurements which have been conducted so far were the stiffness for a horizontal force applied to the center of gravity of the lower platform suspension plane and the stiffness for a moment about the vertical axis applied to the same platform. Figure 5 shows the force versus displacement plot from the first case superimposed to the theoretical model predicted plot. Figure 6 shows the moment versus angular displacement plot from the second case superimposed to the theoretical model predicted plot.

In the first case the theoretical model predicted stiffness averaged 14.6% less than that measured by the experiment. In the second case the theoretical model predicted stiffness averaged 33.8% less than that measured by the experiment. At present, the wireropes have been replaced with new ones of 3/4-in diameter and a more thorough investigation of this discrepancy is planned.

4.2 Task II

The objective of this task was the formulation and study of the proposed robot crane suspension stiffness optimization problem and to determine whether there are design rules for the maximization of the stiffness to external loading.

The optimization problem studied was the following. Determine the optimum combination of the dimensions of the upper and lower platform of the proposed robot crane suspension mechanism, which maximize its stiffness for practical values of the total suspended weight, crane height, and diameter of the steel wireropes. In other words, assuming that a given payload has to be delivered to a location of a given height, determine the robot crane design which will maximize its stiffness.

The stiffness matrix of the suspension mechanism for small displacements of the lower platform is given by eqs (2) and (3) of [Unger, J., et al.,1988]. This matrix relates the three-dimensional space forces and moments applied to the center of gravity of the lower platform suspension plane (formed by the three suspension points) with the resulting translations and rotations.

The stiffness functions are as follows:

1. The stiffness K_5 to a single external moment about the vertical axis, given by eqs (3) and (4) of [Unger, J., et al.,1988].
2. The stiffness K_θ to a single external moment about a horizontal axis, given by eq (6) of [Unger, J., et al.,1988].
3. The stiffness K_x to a single external force about a horizontal axis, given by eq (5) of [Unger, J., et al.,1988].

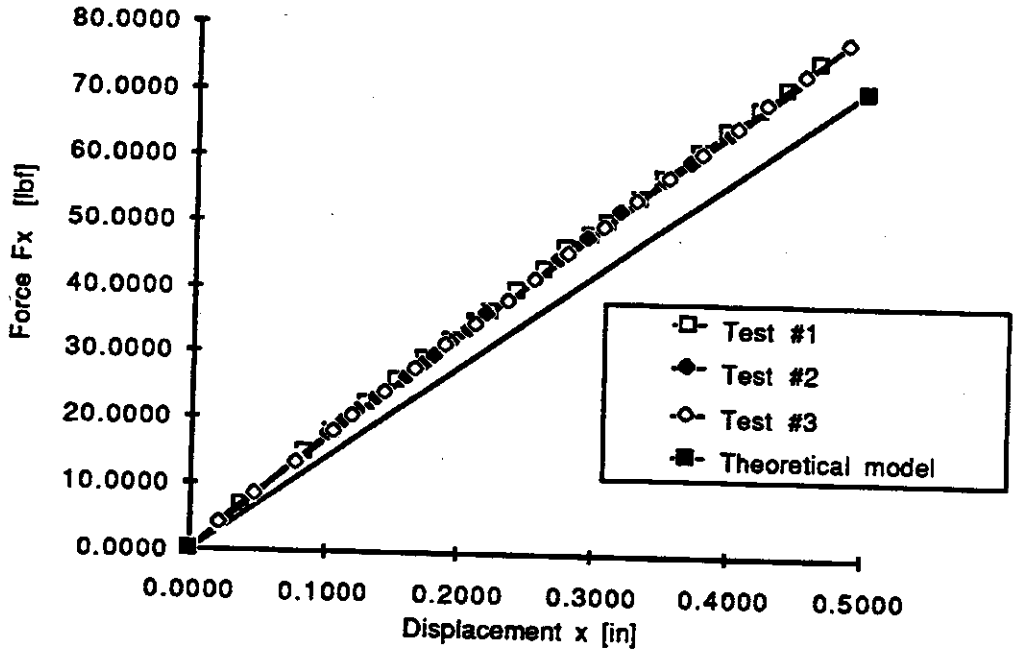

Figure 5. Robot crane force-displacement test results.

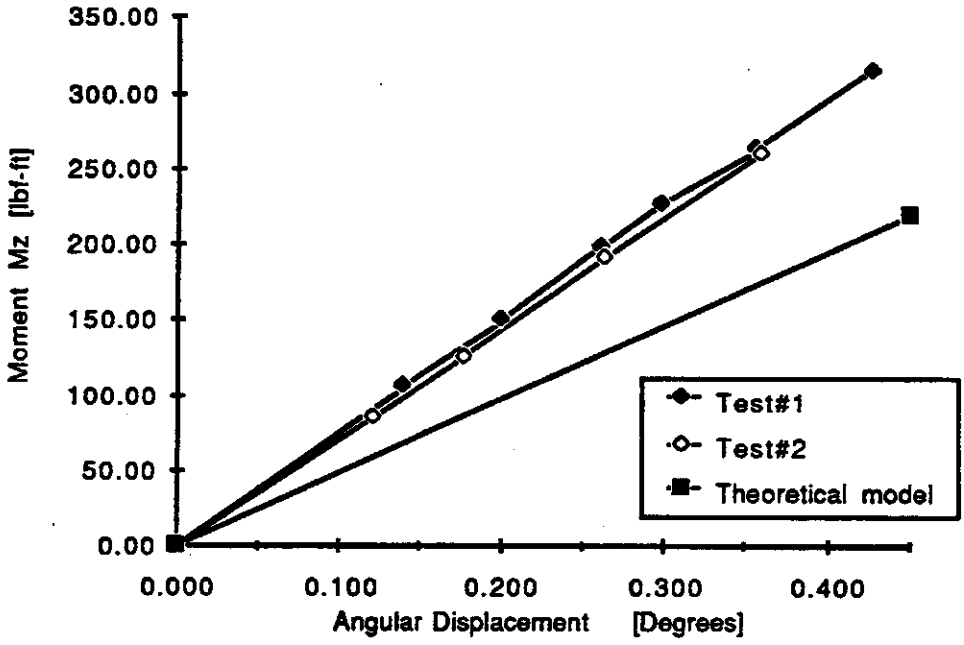

Figure 6. Robot crane moment-angular displacement test results.

4. The stiffness K_3 to a single external force about the vertical axis, given by eqs (3) and (4) of [Unger, J., et al.,1988].

The optimization properties of these functions were studied using optimization searching techniques software programs and exhaustive search computer simulation and plotting programs. The first type of programs used function gradient information to search for optima. The second type of programs were used to gain a better understanding of the behavior of the functions and to check the results of the first. Two different types of analyses were performed, the global maximum analysis and the local maximum analysis. In the first case the relative maxima of the previously mentioned stiffness functions were located for a wide range of payloads and heights. In the second case the size of the upper platform was fixed and the size of the lower platform which maximizes the same stiffness functions was determined (for more details refer to [Unger, J., et al.,1988]). The stiffness functions considered were linear with respect to the wirerope diameter, and increasing diameter would increase the stiffness without reaching any maximum. The wirerope diameter then was treated as an input parameter during the optimization search and not as an optimization variable.

The results of the optimization search are as follows:

1. The global analysis search of the stiffness K_5 function did not locate any relative maximum in the range of payloads (10,000 to 100,000 lb) and heights (10 to 100 ft) searched.

The local analysis search (for specific sizes of the upper platform) did identify local maxima and minima. Figure 7 shows a typical plot of the stiffness function versus the size of the lower platform, from the local analysis search. Where A and B are equal to one-half the side length of the lower and upper equilateral triangle crane platforms respectively. The Young's modulus E and area refer to the modulus of elasticity and effective cross sectional area of the selected wirerope. An area of 0.057 in ^{2} corresponds to a wirerope diameter of 3/8 in. From this figure it can be seen that the stiffness K_5 is equal to zero when A is equal to zero. As A increases the stiffness increases reaching first a local maximum and then a local minimum; beyond that the stiffness keeps increasing as A increases. For practical applications where A cannot exceed 10 to 20 ft this plot can be used to select A, which maximizes the suspension stiffness to a single external moment about the vertical axis.

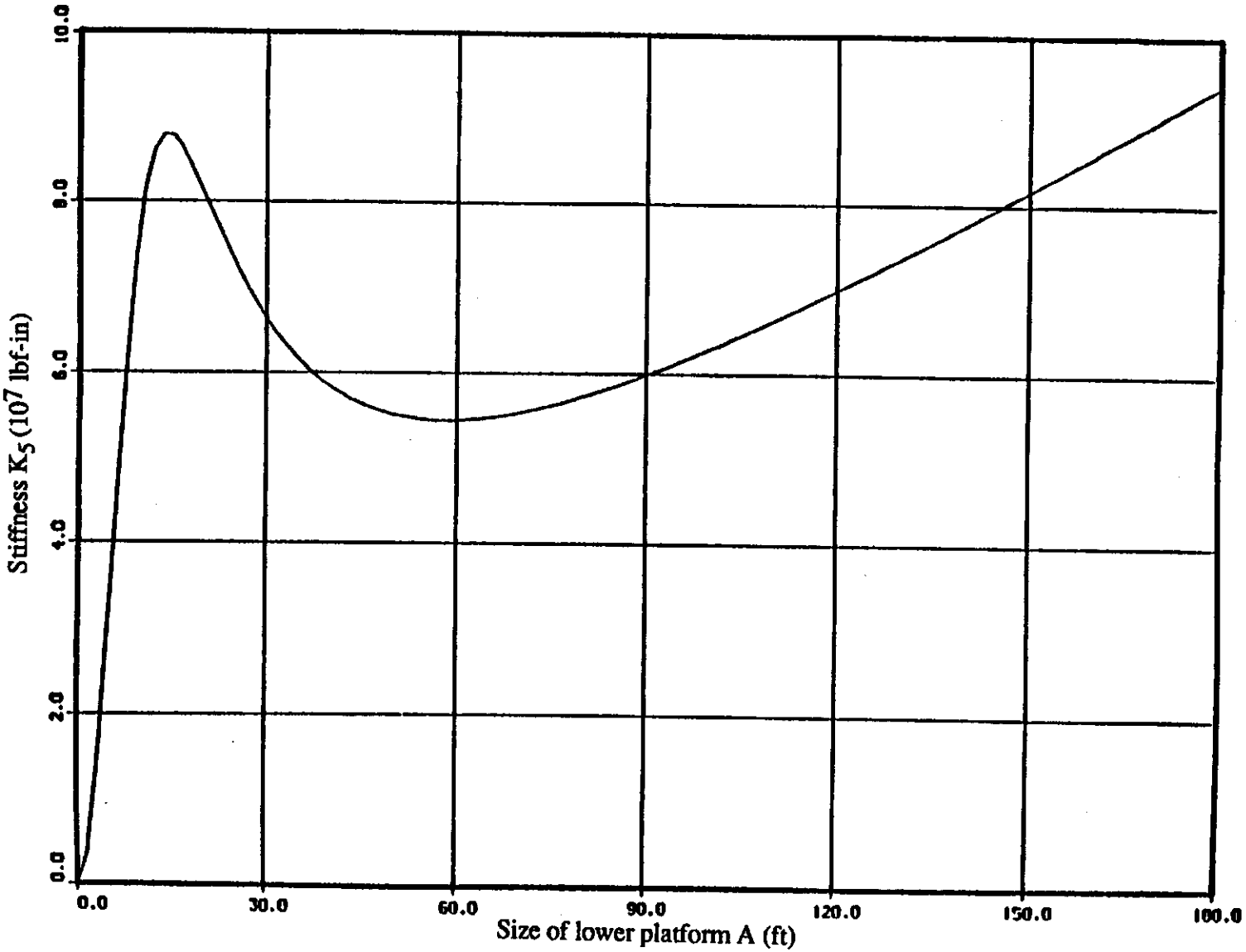

Figure 7. Young's modulus E = 1.08 x 10^7 psi ; Wirerope area = 0.057 in^2
Size of upper platform B = 6 ft ; Weight W = 100 Klbf ; Height H = 10 ft

2. The global analysis search of the stiffness K_θ function did locate a relative maximum in the range of payloads (10,000 to 100,000 lb) and heights (10 to 100 ft) searched. This maximum is achieved when the ratios A/H and B/H take a specific value which ranges from approximately 1.2 to 1.5 for a payload range from 10,000 to 100,000 lb and wirerope diameter from 3/8 to 3/4 in, where H is the crane height. Although the value of the stiffness at that maximum is quite high the resulting design is not very practical for crane applications since it would require very large size upper and lower platforms (large A and B) for any H of practical significance.

The local analysis search (for specific sizes of the upper platform) did identify local maxima and minima. Figure 8 shows a typical plot of the stiffness function versus the size of the lower platform, from the local analysis search. From this figure it can be seen that the stiffness K_θ is equal to zero when A is equal to zero. As A increases the stiffness increases reaching first a local maximum and then a local minimum beyond that the stiffness keeps increasing as A increases. For practical applications, where A cannot exceed 10 to 20 ft, this plot can be used to select A which maximizes the suspension stiffness to a single external moment about a horizontal axis.

3. The global analysis search of the stiffness K_X function did locate a relative maximum in the range of payloads (10,000 to 100,000 lb) and heights (10 to 100 ft) searched. This maximum is achieved when the ratios A/H = 0.707 and B/H = 1.414 and the corresponding value of the stiffness is

$$K_X^* = \frac{\frac{2}{\sqrt{3}} AE + W}{H}$$

where A is the effective cross sectional area of the wirerope, E its Young's modulus of elasticity, and W the total suspended weight. Unfortunately the resulting design is, again, not very practical for crane applications since it would require very large size upper and lower platforms (large A and B) for any H of practical significance.

The local analysis search (for specific sizes of the upper platform) did identify local maxima and minima. From eq (11) of [Unger, J., et al.,1988] it can be seen that K_X has always an optimum, either a maximum or a minimum, when the lower platform is one-half the size of the upper platform (A = B/2), and the corresponding value of the stiffness is

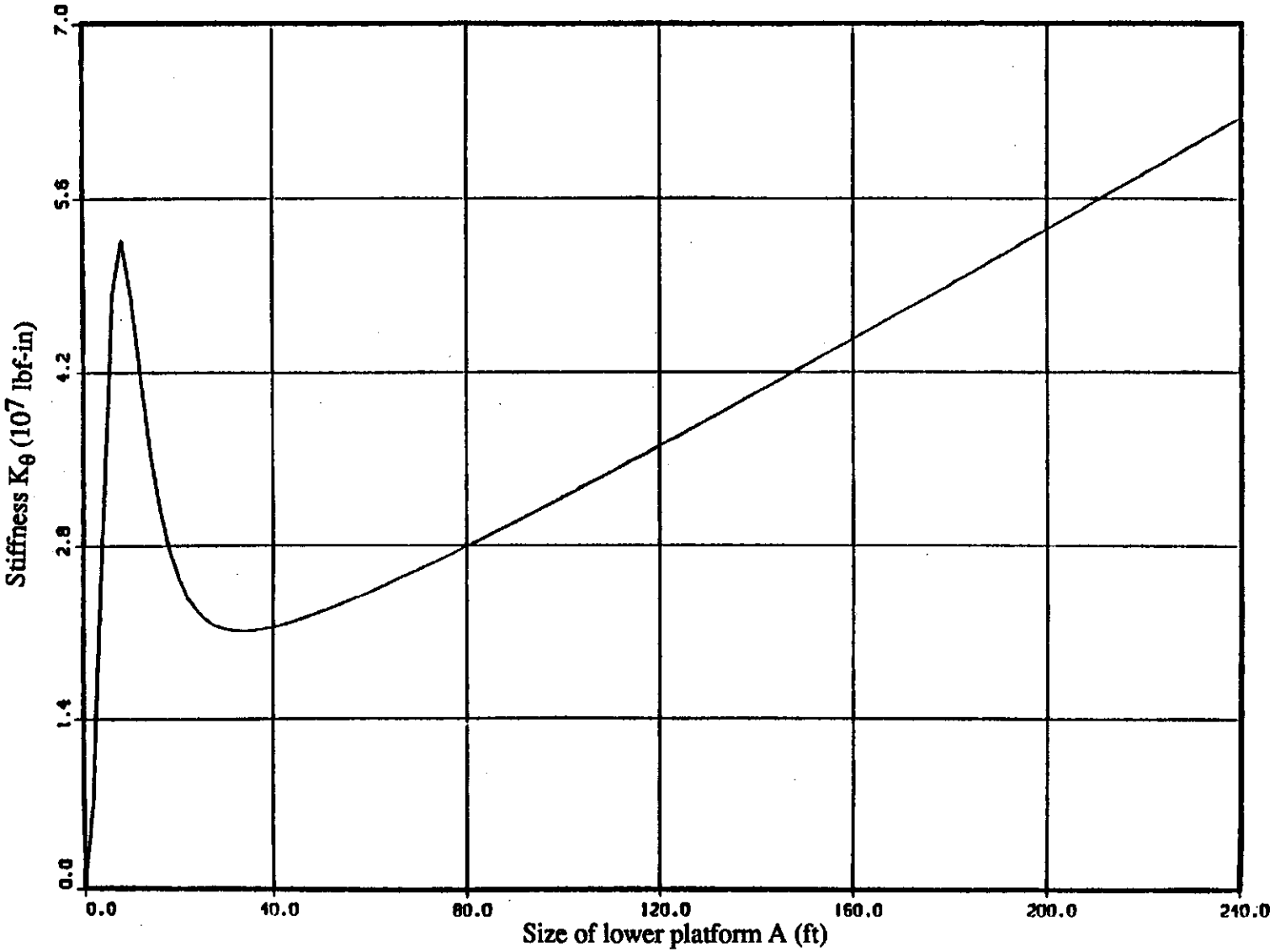

Figure 8. Young's modulus E = 1.08 x 10^7 psi ; Wirerope area = 0.057 in^2
Size of upper platform B = 6 ft ; Weight W = 100 Klbf ; Height H = 10 ft

$$K_X^* = \frac{3AEB^2}{(H^2+B^2)^{3/2}} + \frac{W}{H}.$$

Figure 9 shows a typical plot of the stiffness function versus the size of the lower platform, from the local analysis search. From this figure it can be seen that the stiffness K_X reaches a maximum when A is equal to zero. This corresponds to the case of an inverted pyramid suspended from its base, which is very stiff to a single external force about a horizontal axis applied at its peak. Unfortunately this is not a realistic design because the stiffness to any moment applied to the lower platform would be zero as we saw previously. The maximum at A = 0 on figure 9 follows a local minimum and a local maximum at A = B/2. By varying the values of the payload, height and wirerope diameter it is possible to result in the movement of the maximum towards higher values of A and its replacement by a minimum at A = B/2 as can be seen from figures 2 and 3 of [Unger, J., et al.,1988]. To select the proper A then the value of K_X for the smallest possible A will have to be compared with that of the local maximum and the largest of the two used for the selection of A, which will be used for the actual design.

4. The global analysis search of the stiffness K_3 function did locate a relative maximum in the range of payloads (10,000 to 100,000 lb) and heights (10 to 100 ft) searched. This maximum is achieved when A = B = 0 and it is not a realistic design because the stiffness to any moment applied to the lower platform would be zero as we saw previously.

The local analysis search (for specific sizes of the upper platform) did identify a local maximum when the lower platform is one-half the size of the upper platform (A = B/2), and the corresponding value of the stiffness is

$$K_3^* = \frac{6AEH^2}{(H^2+B^2)^{3/2}} + \frac{W}{H}.$$

Figure 10 shows a typical plot of the stiffness function versus the size of the lower platform, from the local analysis search.

From the optimization results discussed so far it is obvious that the selection of the maximum stiffness design depends on the type of external forces and moments which are expected to dominate the loading of the lower crane platform during actual operation. To help with the selection of the proper design we have tabulated the results of the computer optimization searches

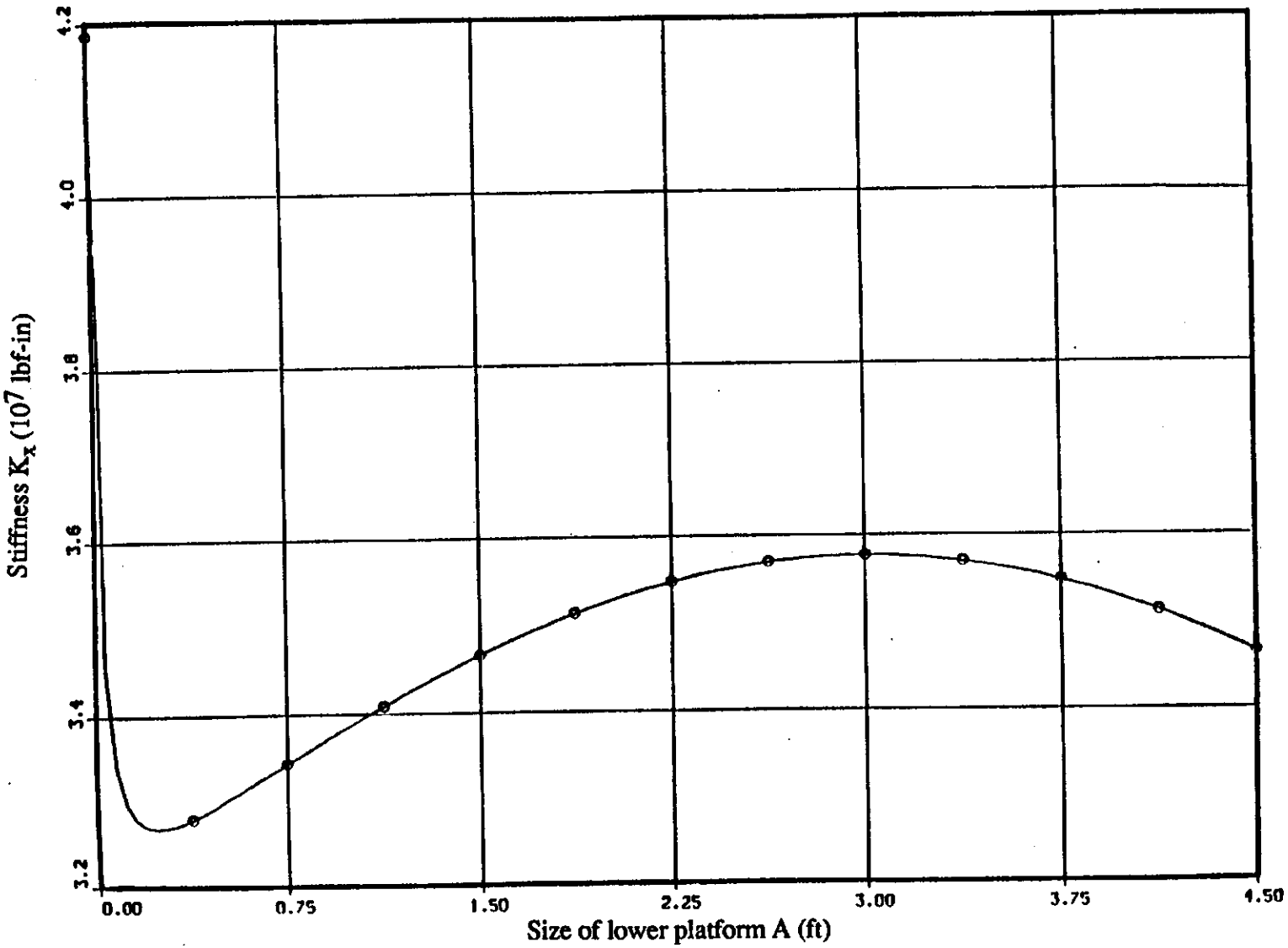

Figure 9. Young's modulus E = 1.08 x 10^7 psi ; Wirerope area = 0.057 in^2
Size of upper platform B = 6 ft ; Weight W = 100 Klbf ; Height H = 10 ft

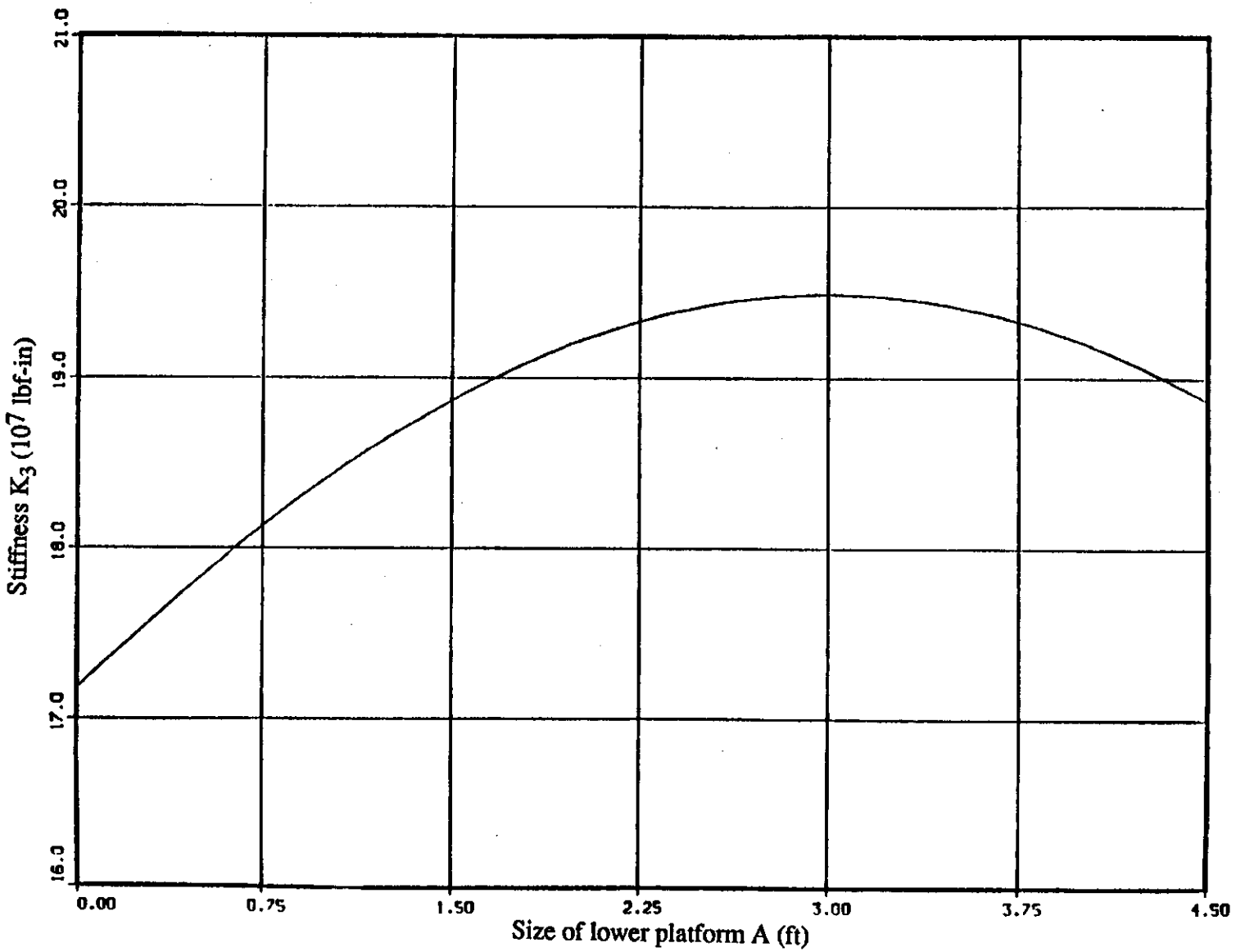

Figure 10. Young's modulus E = 1.08 x 10^7 psi ; Wirerope area = 0.057 in^2
Size of upper platform B = 6 ft ; Weight W = 100 Klbf ; Height H = 10 ft

for three different wirerope diameters (3/8, 9/16, 3/4 in), for a range of payloads from 10,000 to 100,000 lb in increments of 10,000 lb and heights from 10 to 100 ft in increments of 10 ft.

4.3 Task III

The objective of this task was the construction and preliminary testing of a vibration compensation device to damp the oscillations of the payload suspended from the lower platform of the crane.

A small model of the proposed robot crane, shown in figure 11, was constructed for this task. Its upper and lower platforms were two triangular aluminum plates which had the same size. The length of the side of the equilateral triangle platforms was 9 in (A = B = 4.5 in). Six steel wires of 0.042-in diameter were used to suspend the lower platform from a height of approximately 4 ft. This model was equipped with a lateral translation end-load outfitting subplatform model structure (a more detail description of this design is given in [Albus, J., et al., in the press] and figs. 6 and 7). The subplatform structure was modelled with a 2×1 in cross section, 6-ft long steel beam. Two baskets were suspended from its ends for the placement of lead bricks. The front-end basket simulated the payload and the rear end basket the counter weight.

The vibration compensation device used for these tests consisted of a servo-driven x-y table and rotary joint. This device was suspended from the lower platform of the small model robot crane so that it was positioned between the platform and the steel beam (see schematic in fig. 11). In a sense this was a three degrees-of-freedom serial micro-positioner manipulator suspended from the lower platform. With this device it is possible to translate the payload on a plane parallel to that of the lower platform and to rotate it about an axis orthogonal to the same plane. Although these are only three of the degrees-of-freedom that the payload has, they represent the ones with the largest amplitude of oscillations for this design.

The translation and rotation of the payload was measured by three Linear Voltage Differential Transformers (LVDTs), which were fixed horizontal on the floor and were positioned as shown in figure 11. The LVDT transducers measure the displacement of the moving core of their electromagnet and produce an analog voltage signal which corresponds to its absolute position. The tip of the moving core of each of these LVDT sensors was in contact with the steel beam so that it could follow the horizontal component of the low frequency oscillations of the beam. Considering only small amplitude oscillations of the lower platform it was assumed that the motion

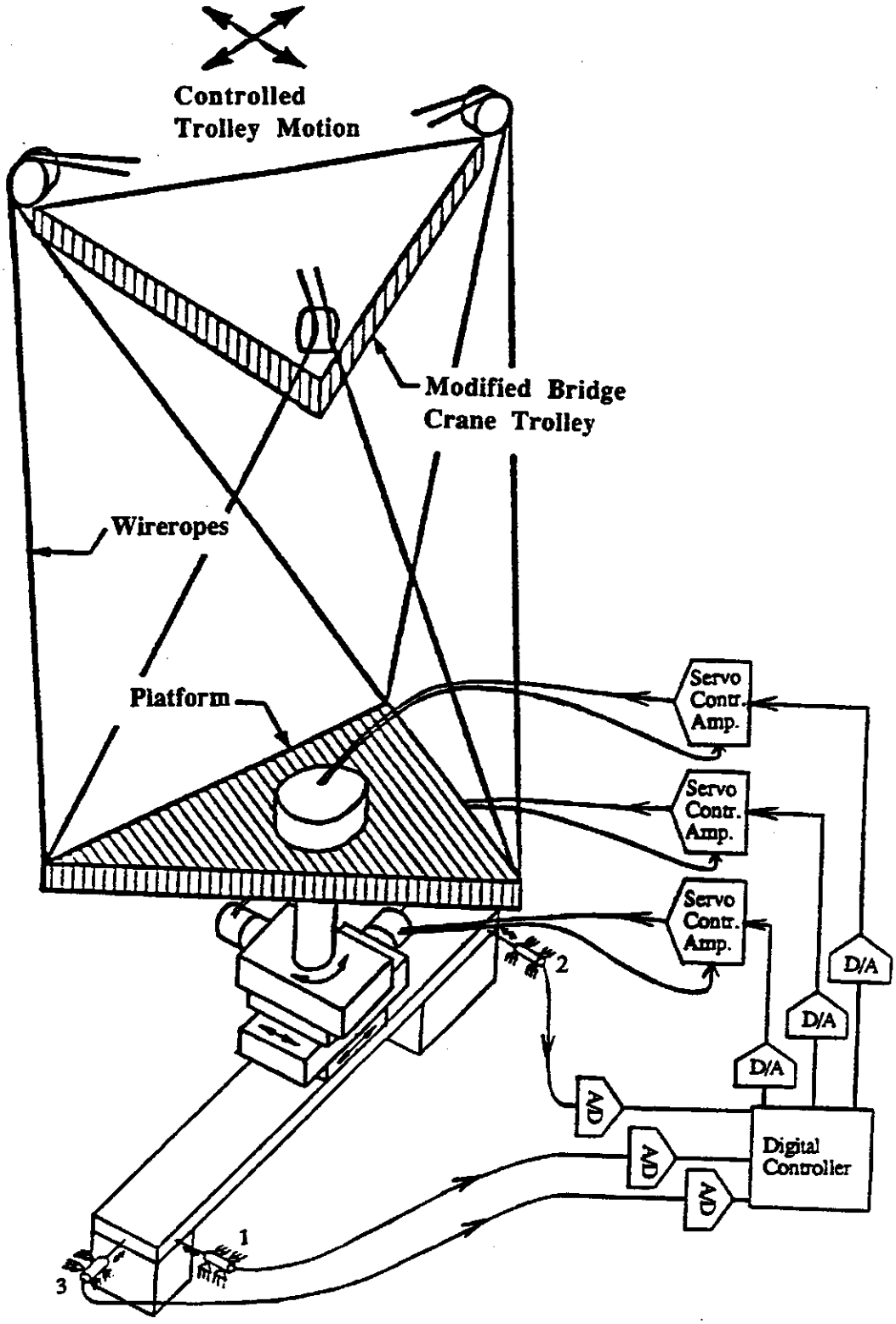

Figure 11. Schematic of the vibration compensation system.

of the steel beam can be approximated by a translation on a horizontal plane and a rotation about a vertical axis.

The outputs of the three LVDT displacement transducers were digitized and sent to an IBM-AT/PC computer which served as a digital controller. The digitized signals were processed by the digital controller to determine the horizontal translation and the vertical axis angular rotation of the steel beam with respect to a reference frame fixed on the floor. Based on that information the necessary amount of translation and rotation of the vibration compensation device is determined, which will bring the payload back to its original position. This information is then processed by a control algorithm which determines the proper command signals to be sent to the three servo drives. A detailed description of these algorithms is provided in Appendix I.

After the electrical and electronic circuitry of the vibration compensation device was completed (see schematic of fig. 12) and tested, the three servo-drives were tuned for optimum response to simple step input command signals from the digital controller. The first digital controller algorithm to be tested was a simple proportional controller. Each of the required displacements of the three axes of the vibration compensator was multiplied with a constant and sent to the servo-drive controllers. The value of that constant was determined experimentally so that each axis has the fastest response possible to an impulse excitation, with no more than two oscillations before reaching steady state.

Figure 13 shows the response of the vibration compensator to an impulse excitation along the longitudinal axis (x-axis) of the steel beam with no digital controller action. Figure 14 shows the response to a similar excitation with digital control action. Figure 15 shows the response of the vibration compensator to an impulse excitation orthogonal to the longitudinal axis (y-axis) of the steel beam with no digital controller action. Figure 16 shows the response to a similar excitation with digital control action. Figure 17 shows the response of the vibration compensator to an impulse moment excitation along the vertical axis (z-axis) of the steel beam with no digital controller action. Figure 18 shows the response to a similar excitation with digital control action.

As can be seen from these test results there is a significant improvement in the response of the payload of the robot crane model to horizontal force excitation inputs, but not in the response to moments about the vertical axis. An increase in the digital controller gain of that axis leads to more oscillatory response and eventually instability. This points to the need to use more sophisticated controller algorithms, at least for that last axis.

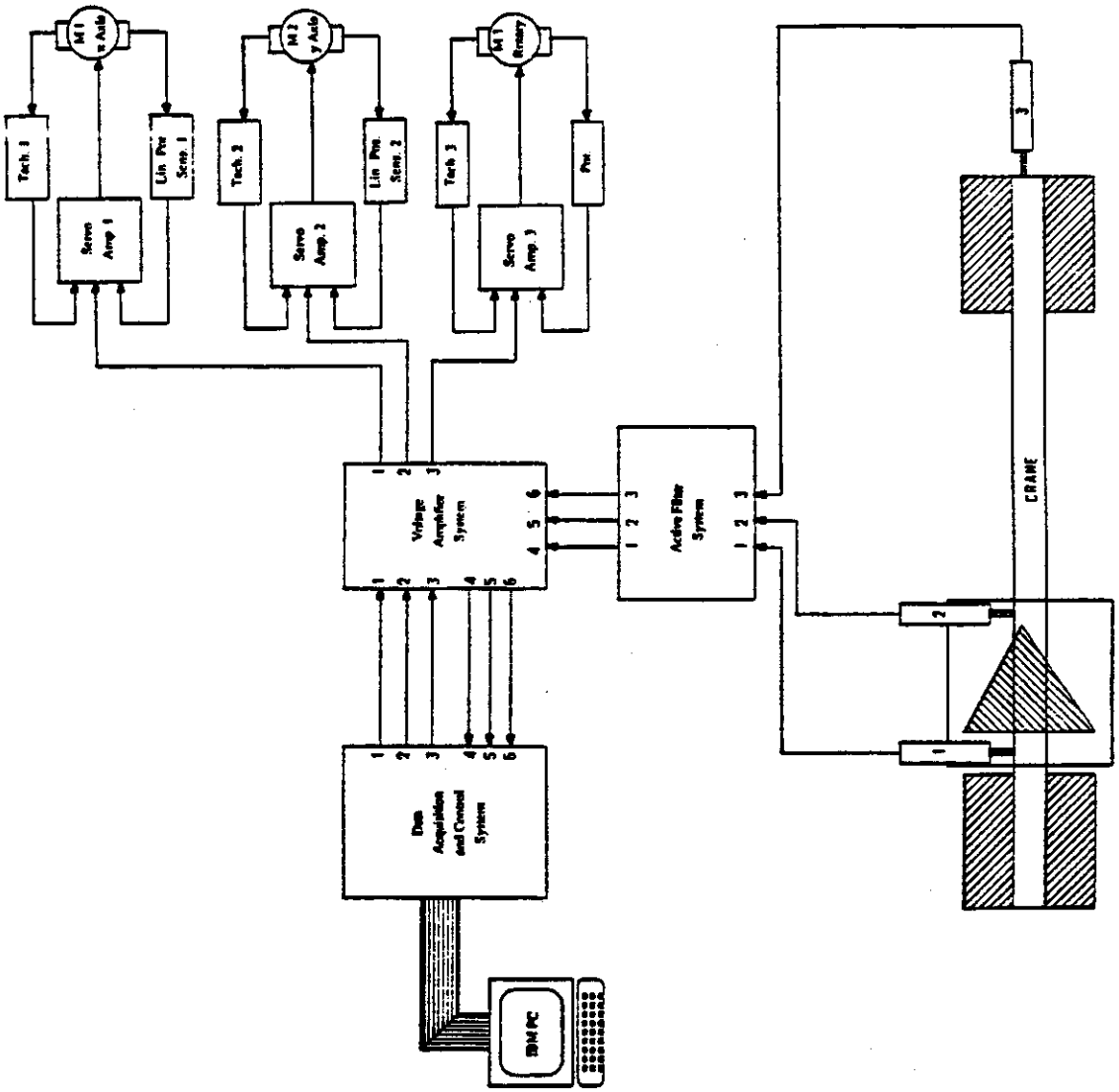

Figure 12. Schematic of the electrical and electronic circuitry.

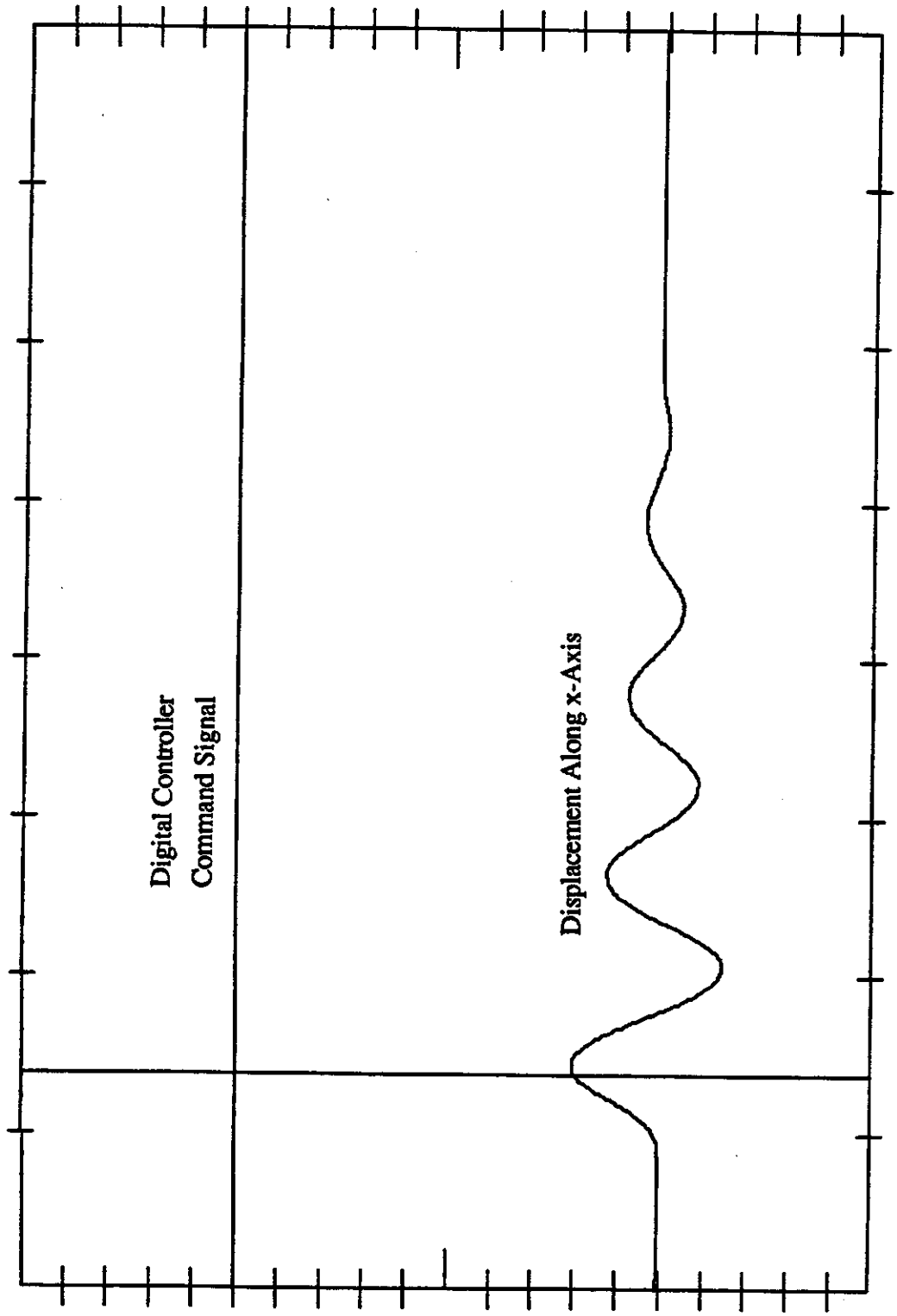

Figure 13. Response of the vibration compensator.

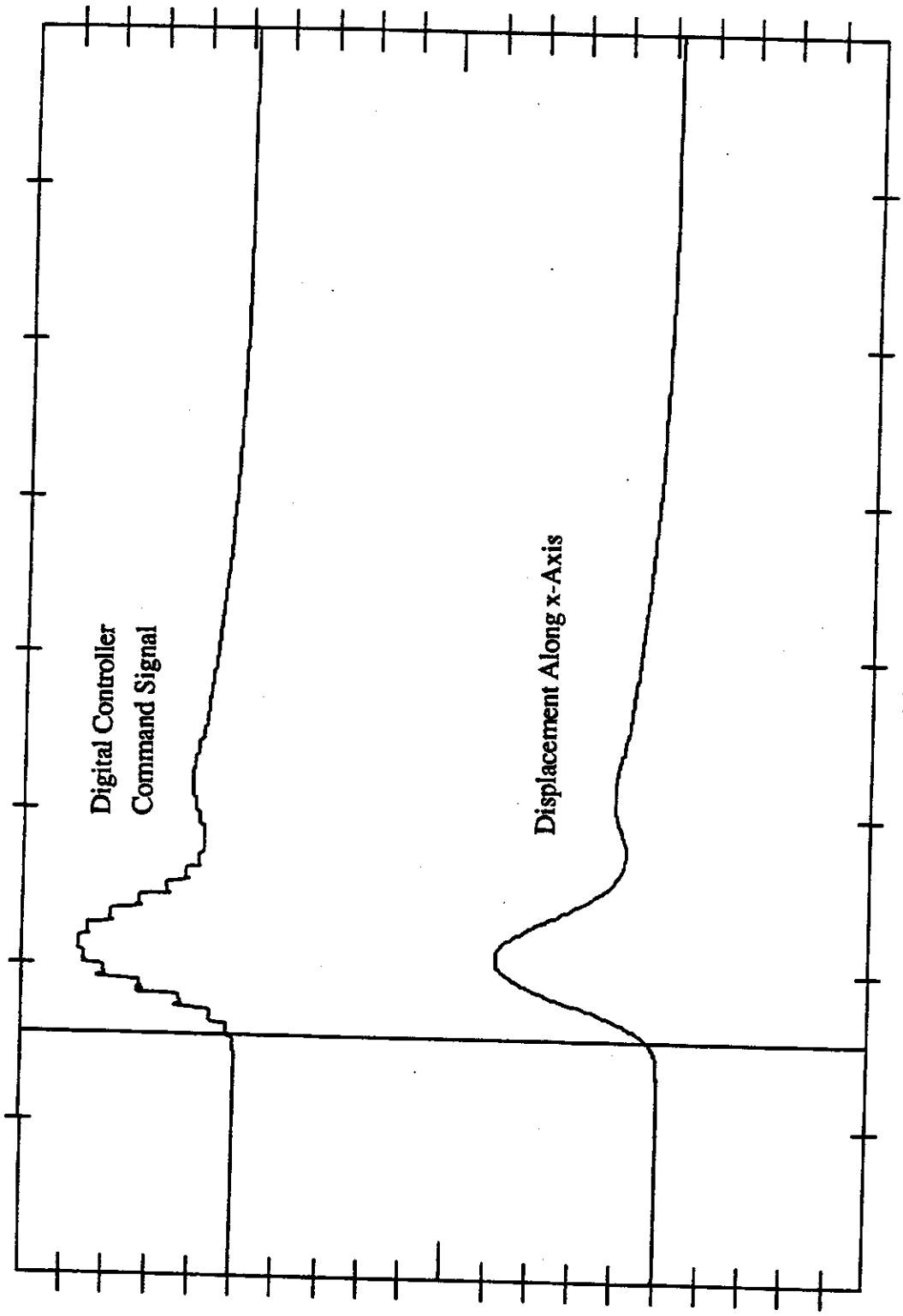

Figure 14. Response of the vibration compensator.

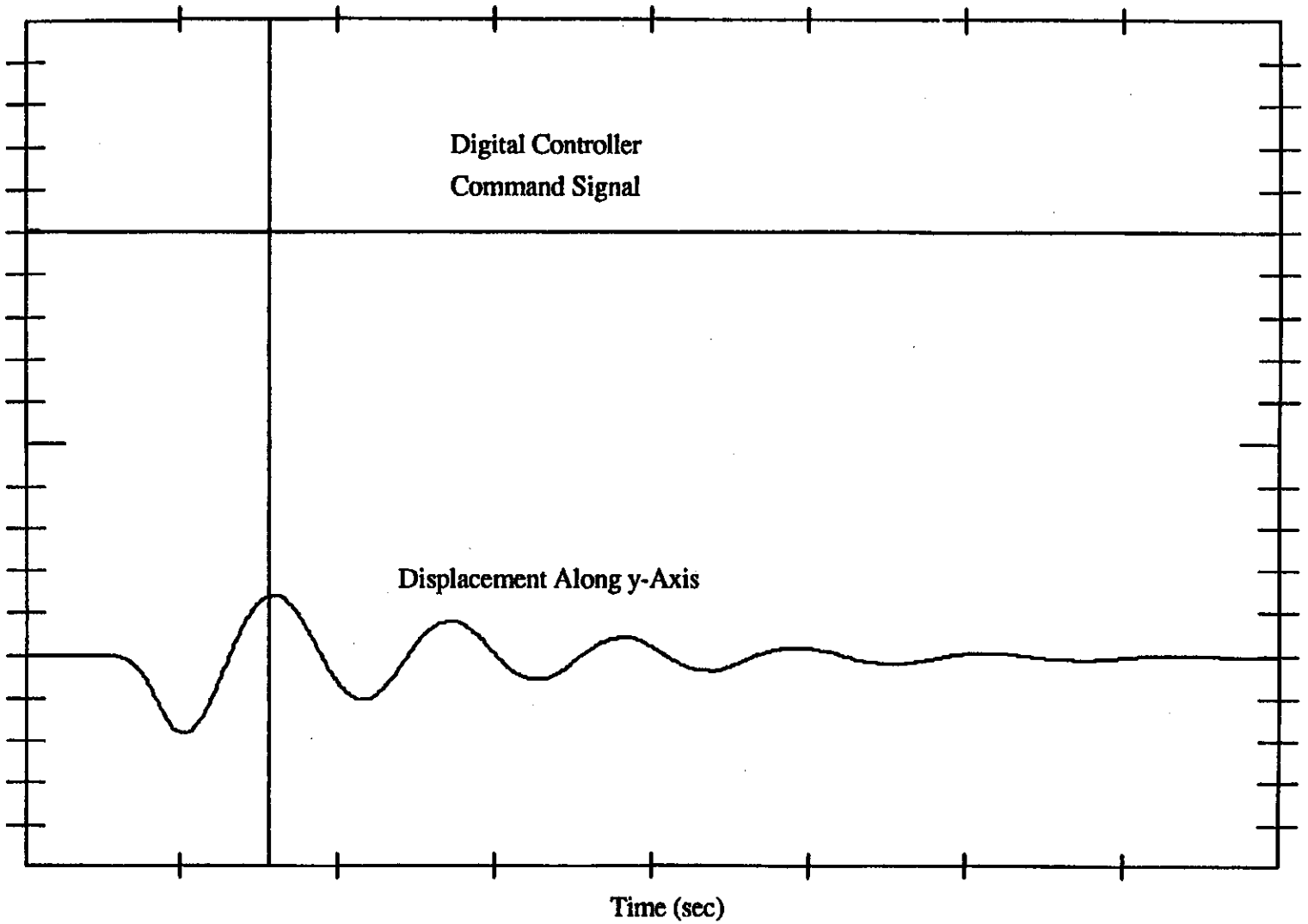

Figure 15. Response of the vibration compensator.

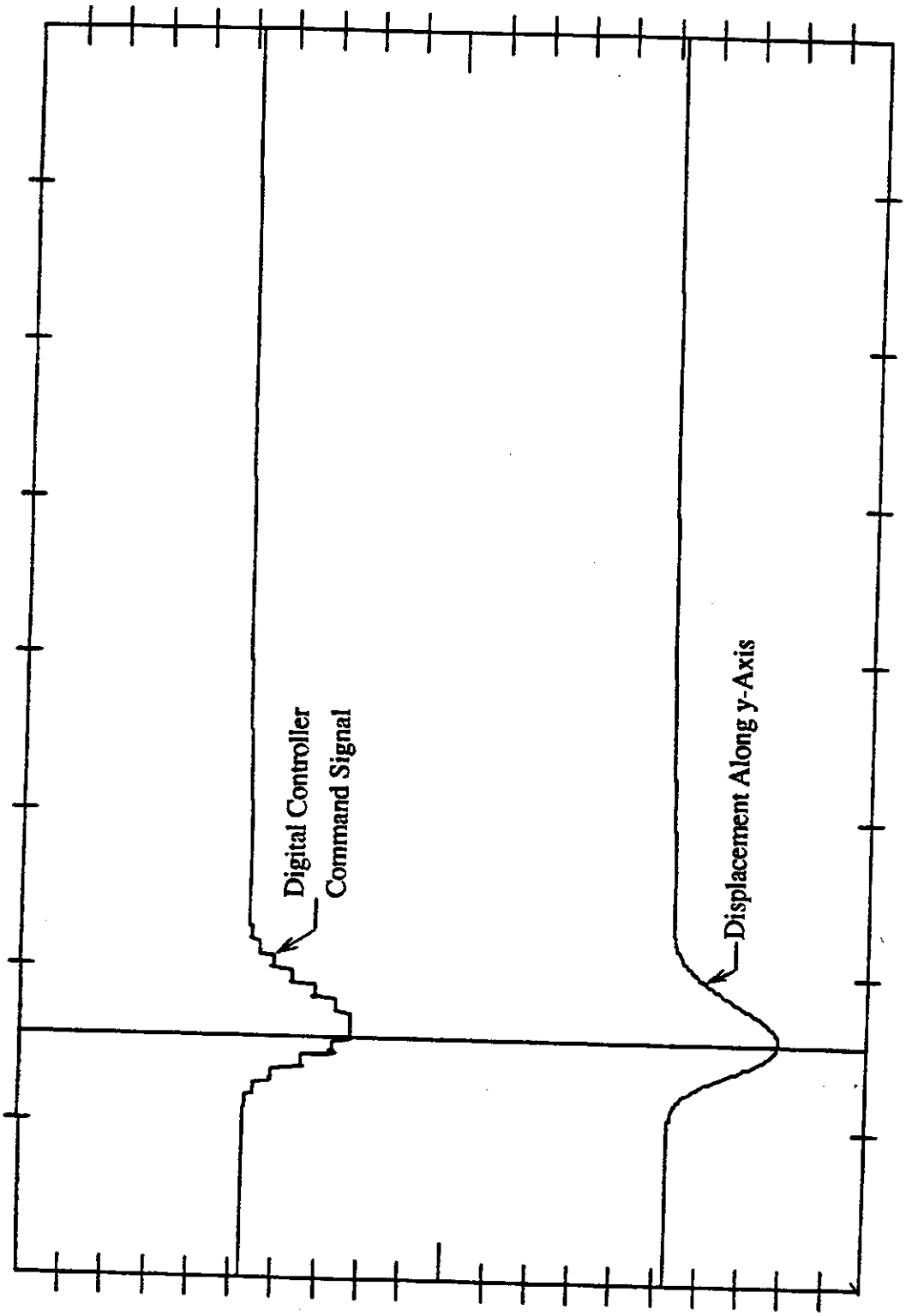

Figure 16. Response of the vibration compensator.

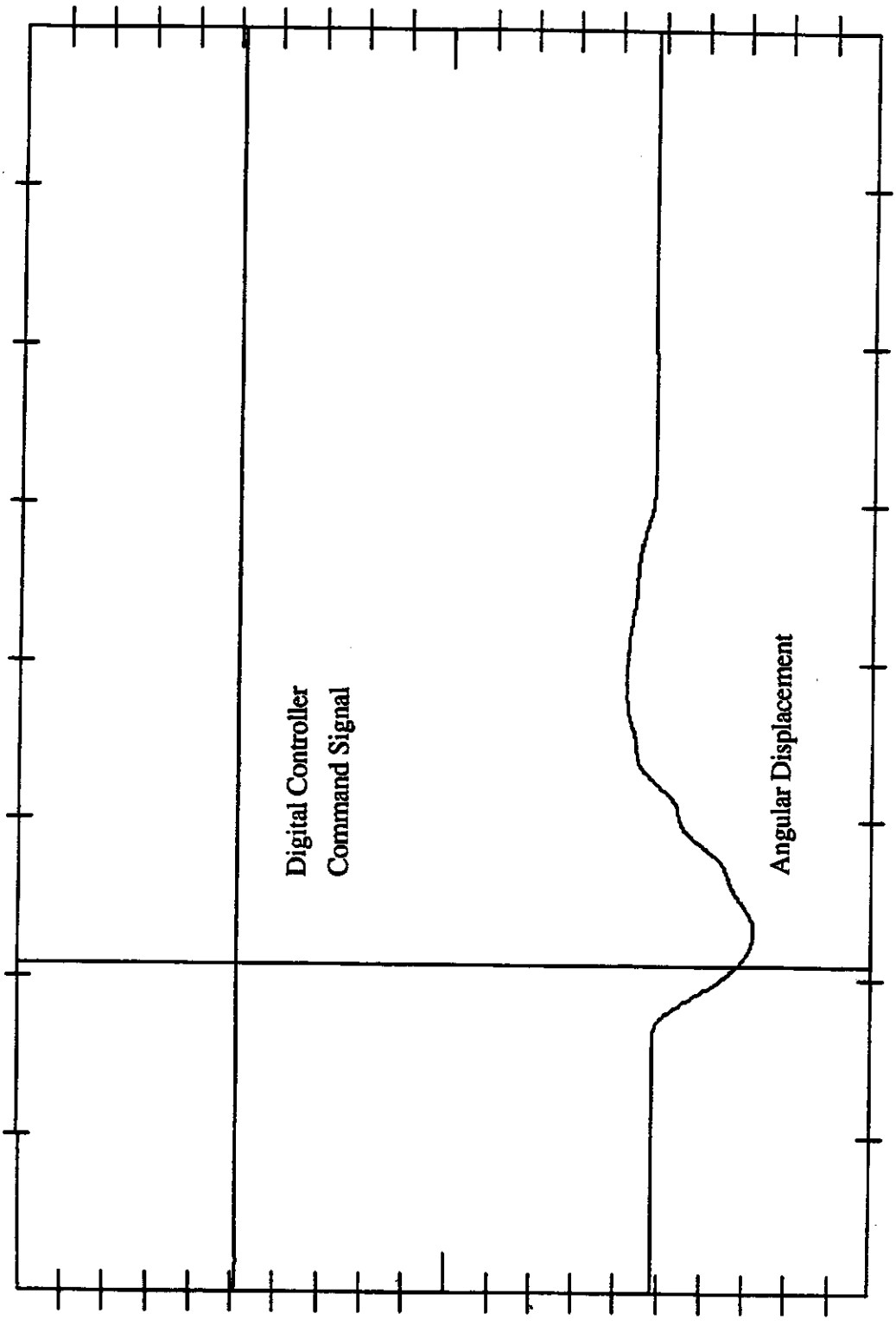

Figure 17. Response of the vibration compensator.

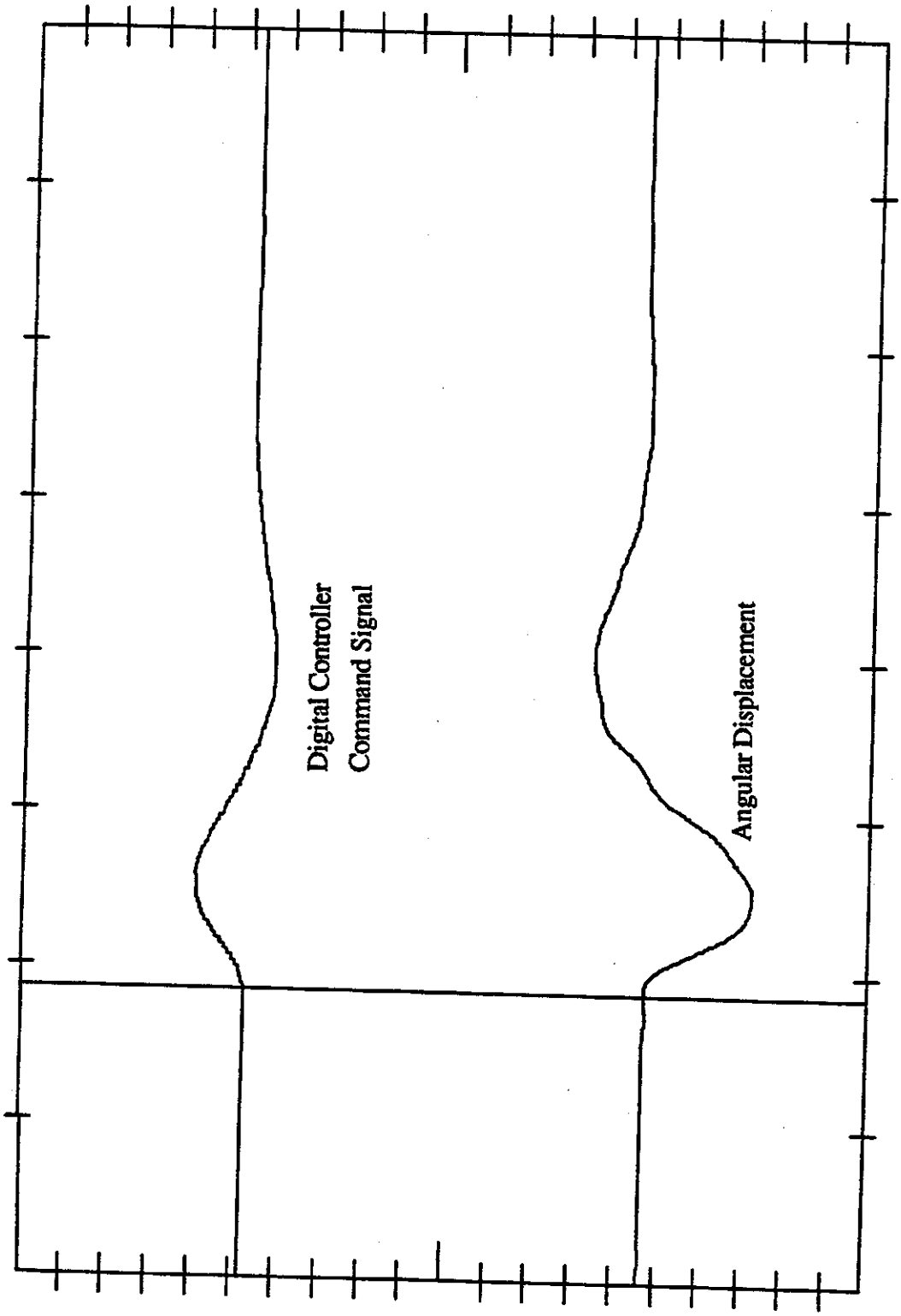

Figure 18. Response of the vibration compensator.

4.4 Task IV

The objective of this task was to construct an intermediate-size robot crane model for factory automation use. Suspend a robot arm from the lower crane platform, as shown in figure 2, and demonstrate the capability to monitor the position of the robot arm end-effector, as it moves in three-dimensional space, with noncontact sensors.

The largest size upper platform which could be suspended from the ceiling of our lab, without the wireropes interfering with the light fixtures, was an equilateral triangle of 6-ft long side (B = 3 ft). The diameter of the wireropes was selected to be 3/8 in. The height 12 ft 8 in was selected to allow enough clearance between the robot arm end-effector and the floor. A PUMA-560 robot arm which became available for this task weighs approximately 150 lb with its end-effector. This allows us to suspend several hundred pounds of payload from the lower platform in addition to the robot arm.

Since the robot arm is relatively short and has low manipulation power, no significant moments were expected to be developed on the lower crane platform during its operation. Thus it was decided to build a crane suspension system which is stiff to external forces rather than moments. Based on the results of the optimization analysis that design could be achieved with a lower platform which is one-half that of the upper platform (A =B/2 = 1.5 ft). Figure 19 shows a picture of the intermediate-size model with the robot arm hanging underneath.

This type of robot crane design can be used for the automation of industrial operations. If the upper platform is mounted on the carriage of a gantry crane the robot arm can be used to load and unload several machine tools. Compared to the current practice of using dedicated robot arms to load and unload machine tools this design could reduce the number of needed robots and free valuable factory floor space for other use. By hanging a hook underneath the lower platform, as shown in figure 2, heavy parts and fixtures can be moved, and with the help of the robot arm be accurately positioned. By mounting drills, deburring tools, etc., from the lower platform, the lateral stiffness capability of the crane suspension can be used to do drilling, deburring, etc., on sheet metal structures while the robot arm could hold vision or touch sensors to assist with the machining operation. Similarly, vision or other sensors could be used for the inspection of large structures, such as airplanes, ships, etc.

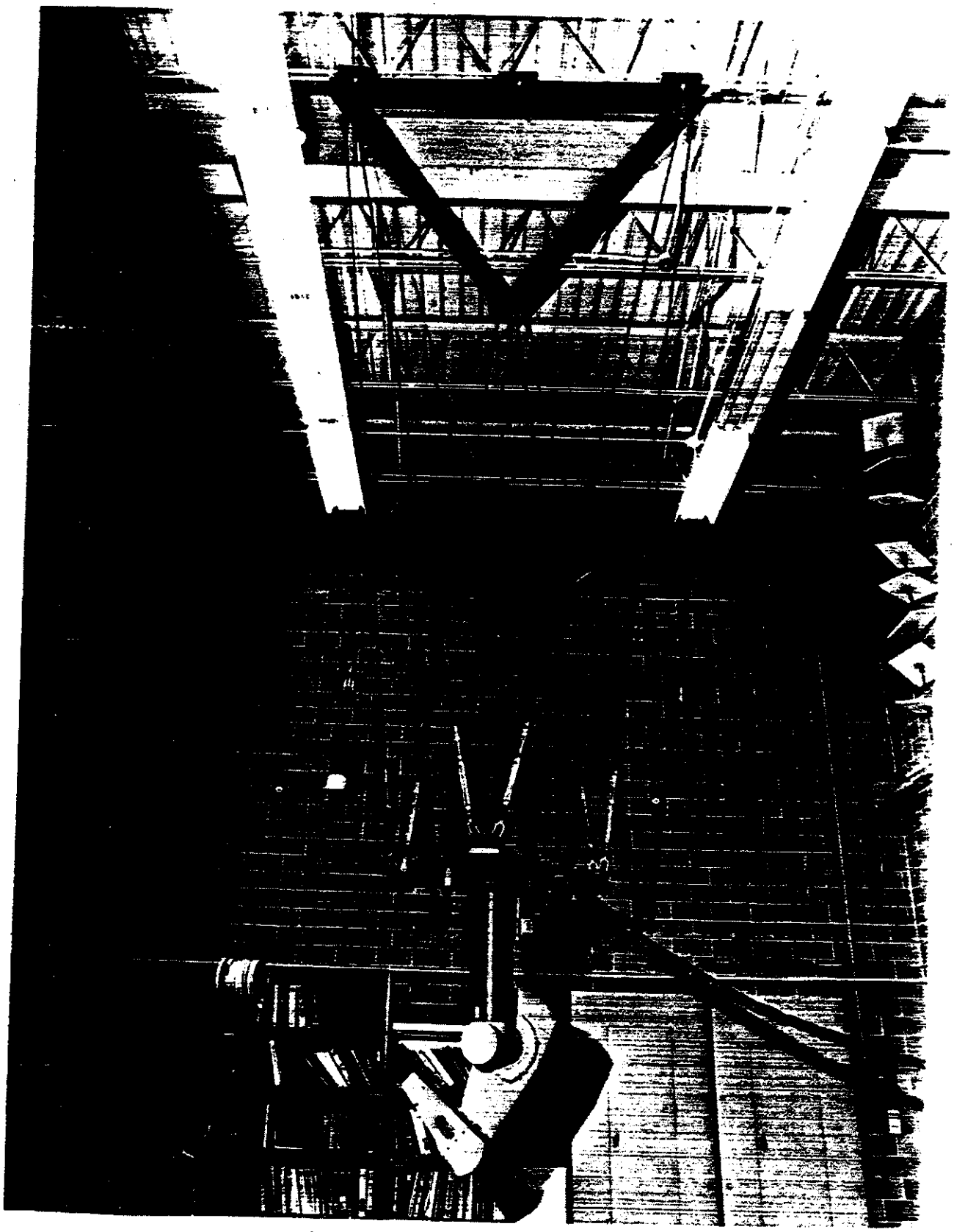

Figure 19. Intermediate size model.

To demonstrate the capability to monitor the movement of the robot arm in three-dimensional space while hanging underneath the crane lower platform we used the newly completed Robot Laser Tracker interferometer which was developed at NIST jointly by our Division and the Precision Engineering Division [Lau, K., et. al., 1985]. This instrument measures the spherical coordinates of a retroreflecting optical target which is mounted on the moving body to be monitored. It shoots a laser beam to the target which is then used by an interferometer to measure the change in the distance between the target and a mirror at the head of the instrument. When the target moves the mirror is servoed to follow it. Two precision encoders measure the azimuth and zenith angles of the mirror. The distance and angle information is then combined to determine the x, y, z position of the optical center of the target with respect to the coordinate system of the Robot Laser Tracker interferometer. Figure 20 shows a picture of the Robot Laser Tracker following the optical target mounted at the end-plate of the PUMA-560 arm. Figure 21 shows a three-dimensional plot of the optical target trajectory as the robot is commanded to follow the standard test path proposed to the American National Standards Institute (ANSI) by the Robotic Industries Association (RIA). Figure 22 shows the same trajectory with respect to a coordinate frame located at the centroid of the trajectory which allows a better observation of details.

Figure 20. Robot Laser Tracker following the PUMA-560 robot arm.

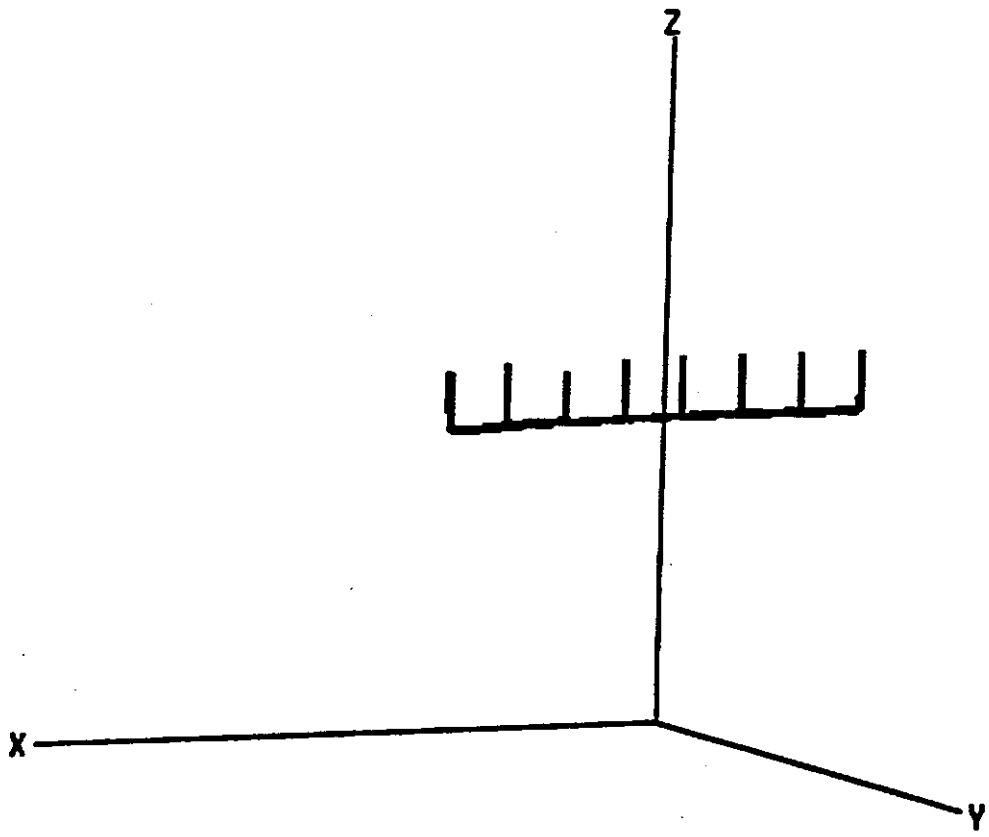

Figure 21. Target trajectory with respect to the Laser Tracker coordinate system.

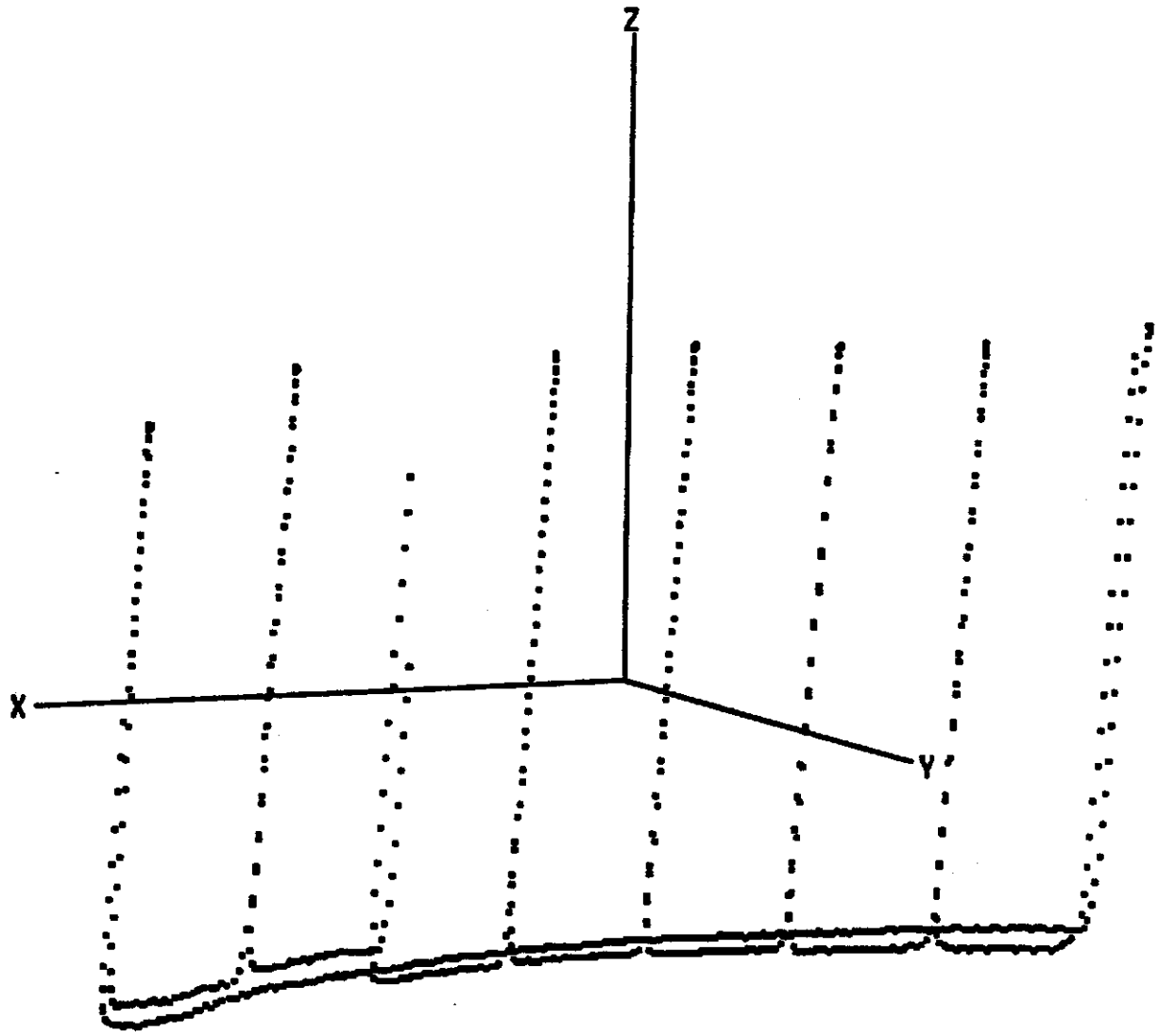

Figure 22. Target trajectory with respect to a centroid coordinate system.

5. Summary and Conclusions

The robot crane technology program has made good progress toward its objective of developing kinematically constrained, dynamically stabilized, robot cranes capable of lifting, moving, and positioning heavy loads, capable of supporting fabrication and construction operations.

Progress in the period from April 1 to November 31, 1988:

* A theoretical model of the proposed robot crane suspension mechanism has been developed and tested with a full-size robot crane model. The stiffness of the crane suspension mechanism of a full-size model was measured for two different types of external loads and compared with the theoretical model predicted values. The full-size model suspension consisted of six wireropes of 3/8-in diameter, which supported a total load of approximately 19,000 lb, from a height of approximately 29 ft. The stiffness to a horizontal external force and the stiffness to a moment about the vertical axis applied to the lower suspended platform were measured. In the first case, the theoretical model predicted stiffness is on the average 14.6% less than that measured by the experiment. In the second case, the theoretical model's predicted stiffness is on the average 33.8% less than that measured by the experiment. At the present the wireropes have been replaced with new ones of 3/4-in diameter and a more thorough investigation of this difference is planned.

* The proposed crane suspension stiffness optimization problem was formulated. The optimization problem was studied for four different external loads. These were an external horizontal force, an external vertical force, a moment about the vertical axis, a moment about a horizontal axis, each of them applied to the lower suspended platform. A global and a local maximum analysis study were conducted and general design rules were formulated. The selection of the maximum stiffness design depends on the type of external forces and moments which are expected to dominate the loading of the lower crane platform. The most convenient way to proceed with the selection of a design is probably to pick a few different sizes of the upper crane platform and then follow the rules described in section 4.2 for the selection of the lower platform size. The combination of the upper and lower platform with the highest stiffness should be the best choice. The results of the optimization search have been tabulated and can be used to facilitate the design process.

* A three degrees-of-freedom robot crane payload vibration compensation device was constructed and tested on a small crane model. This device consisted of a servo-driven horizontal X-Y table and rotary joint about the vertical axis, which was suspended from the model crane lower platform. The oscillations of the payload in the horizontal plane and its rotations about the vertical axis were detected by external sensors and a digital controller determined the appropriate command signals to the servo-drives in order to compensate them. A simple proportional gain digital controller algorithm was used for this stage of the investigation. The gains were selected experimentally in order to minimize the number and amplitude of the oscillations of the payload in the corresponding direction. The payload response to force disturbances along the horizontal plane showed a significant improvement when the vibration compensation control was on. The payload response to moment disturbances about the vertical axis did not show any noticeable improvement when the vibration compensation control was on.

* An intermediate-size model robot crane was constructed for factory automation applications. Its upper platform was an equilateral triangle with a side length of 6 ft. Based on the stiffness optimization study, the lower platform was selected to be one-half the size of the upper platform. A PUMA-560 robot arm was suspended from the lower platform of this model. A robot three-dimensional tracking laser interferometer was used to monitor the movements of the arm in space and software was written to process and display the path tracking data. The robot arm turned out to be quite stiff to any type of external disturbances. Above a certain level though the wireropes would buckle making the arm yield (see fig. 12 of [Dagalakis, N.G., et al., 1988]). This could be a very desirable feature for applications where safety requires that the forces or moments applied by the robot arm do not exceed certain limits.

Proposed future work:

* Theoretical study and measurement of the buckling characteristics of the robot crane suspension mechanism.

* Design and testing of active damping and the micro-positioning control systems of an intermediate scale crane platform.

* Add vision, touch, and force sensors and demonstrate the ability of a robot crane to load and unload machine tools in a factory environment.

* Develop the proper sensors and grippers and demonstrate the ability of a robot crane to pickup and deliver heavy fixtures in a factory environment.

* Develop the proper sensors and grippers and demonstrate the ability of a robot crane to provide lateral support to do drilling, deburring, etc., of large and inaccessible sheet metal structures.

* Retrofit a tower crane, develop the proper sensors and grippers and demonstrate the ability of a robot crane to pickup and deliver heavy payloads of different shapes and sizes for construction work.

6. Acknowledgments

The robot crane technology program was funded by the Defense Advanced Research Projects Agency, Information Science and Technology Office, ARPA order 6380. Dr. Robert L. Resenfeld was the project sponsor.

We would like to acknowledge the help of the following people. Mr. Mitch Tarica for the design and construction of most of the mechanical components used for this work and his help with some of the experiments. Mr. Wendell Wallace for the construction of the vibration compensation electrical system. Mr. Frank Rankin for his help with the construction of the full-size robot crane model.

7. References

Albus, J. S. A stabilized lifting platform. Internal Nat. Bur. Stand. (U.S.) Memo; 1987.

Albus, J. S.; Dagalakis, N. G.; Wang, B-L; Unger, J.; Lee, J. D.; Yancey, C. W. Available robotics technology for applications in heavy industry. To be published by the Iron and Steel Engineer; 1988.

Bennett, W. M. Mechanical wrist for a robot arm. Mech. Eng. Dept. Mass. Inst. of Tech. B.S. Thesis; 1968.

Carbon, L. Automation of grab cranes. Siemens Review 43(2): 80-85; 1976 February.

Dagalakis, N. G.; Albus, J. S.; Wang, B-L; Unger, J.; Lee, J. D. Stiffness study of a parallel link robot crane for shipbuilding applications. Proc. Offshore Mechanics and Arctic Eng. Conf.; 1988 February; Houston, TX.

Fichter, E. F.; McDowell, E.D. A novel design for a robot arm. Proc. Int. Computer Tech. Conf.: 250-256; 1980 August; San Fransisco, CA.

Fichter, E. F. Kinematics of a parallel connection manipulator. ASME Paper 84-DET-45 delivered at the Design Eng. Tech. Conf.; 1984 October; Cambridge, MA.

Fichter, E. F. A Stewart platform based manipulator: General theory and practical construction. The Kinematics of Robot Manipulators, MIT Press: 165-190; 1987.

"Gadfly- the Answer to Electronic Component Assembly," Assembly Automation: 20-22; 1983 February.

Gough, V.E., "Contribution to Discussion of Papers on Research in Auto Stability and Control and in True Performance by Cornell Staff", Proc. Auto Div. Inst. Mech. Eng., pp.392-403, 1956-1957.

Gough, V. E.; Whitehall, S. G. Universal tyre test machine. Proc. 9th Int. Automobile Technical Congress: 117-135; 1962.

Kogure, H.; Tojo, M. Recent developments in crane control. Hitachi Review 27(6): 315-320; 1978.

Koliskor, A. S. Development and investigation of industrial robots based on specification by l-coordinates. Soviet Engineering Research 2(12): 75-78; 1982.

Konstantinov, M. S.; Sotirov, Z. M.; Zamanov, V. B.; Nenchev, D. N. Force Feedback Control of Parallel Topology Manipulating Systems. Proc. 15th Int. Symp. on Industrial Robots: 181-188; 1985 September; Tokyo, Japan.

Kubo, M. Robots and computers to automate Japanese shipbuilding. Keynote address II, 6th Int. Symp. on Offshore Mechanics and Arctic Engineering: 1987 March; Houston, TX.

Landsberger, S. E.; Sheridan, T. B. A new design for parallel link manipulators. Proc. Systems Man and Cybernetics Conf.: 812-814; 1985 November; Tucson, AZ.

Lau, K.; Hocken, R.; Haynes, L. Robot end point sensing using a laser tracking system. Proceedings of the Workshop on Robot Standards: 104-111; 1985 June; Detroit, MI.

McCallion, H.; Johnson, G. R.; Pham, D. T. A compliant device for inserting a peg in a hole. The Industrial Robot : 81-87; 1979 June.

Multicraft A/S; Oslo, Norway.

Powell, I. L. The kinematic analysis and simulation of the parallel topology manipulator. The Marconi Review XLV (226): 121-138; 3rd quarter 1982.

Sheridan, T. B. Human supervisory control of robot systems. Proc. Int. Conf. on Robotics and Automation: 808-812; 1986 April; San Fransisco, CA.

Stewart, D. A platform with six degrees of freedom. Proc. of the Inst. of Mech. Eng. 180(15) Part I: 371-386; 1965-1966.

U. S. Department of Commerce, International Trade Administration. 1987 U.S. Industrial Outlook.

Unger, J.; Dagalakis, N. G.; Tsai, T. M.; Lee, J. D. Optimum stiffness study for a parallel link robot crane under horizontal force. Proceedings of the 2nd Int. Symp. on Robotics and Manufacturing: 1037-1046;1988 November; Albuquerque, NM.

Appendix I

Development of the Vibration Compensation Signal Processing and Control Algorithms

IV.1 The Signal Processing Algorithms

The translation and rotation of the payload was measured by three Linear Voltage Differential Transformers (LVDTs), which were fixed parallel to the floor and were positioned as shown in figure 11 of the main report. The LVDT transducers measure the displacement of the moving core of their electromagnet and produce an analog voltage signal which corresponds to its absolute position.

Figure IV.1 shows the steel beam, which supports the payload and the counterweight (for more details refer to sec. 4.3 of the main report), and the three LVDTs. LVDTs 1 and 2 are positioned parallel to each other with their sensor probe in contact with the same side surface of the beam, while LVDT 3 is oriented with its axis orthogonal to the other two, so that its probe is in contact with another side surface of the beam. To reduce friction the surface of the beam which comes in contact with the LVDT probes was covered with Teflon tape. At the beginning of each test the LVDT sensors were carefully positioned so that they are all at the same horizontal level and the axes of their moving cores are orthogonal to the corresponding side of the beam.

Let (x_b, y_b, z_b) be a coordinate system fixed on the beam with origin located at (x_{cb}, y_{cb}, z_{cb}). The location of the origin (x_{cb}, y_{cb}, z_{cb}) is measured from the absolute reference coordinate system (x, y, z) fixed on the floor.

Any flat surface of the beam can be described by eq

$$a_b x_b + b_b y_b + c_b z_b = d_b \quad , \tag{1}$$

where a_b, b_b, c_b are the directional cosines of the surface normal and d_b is the distance of the surface from the origin x_{cb}, y_{cb}, z_{cb}.

Each LVDT sensor will give the coordinate (x, y, z) of the contact point between the sensor probe and the beam side surface, measured with respect to the absolute reference coordinate frame.

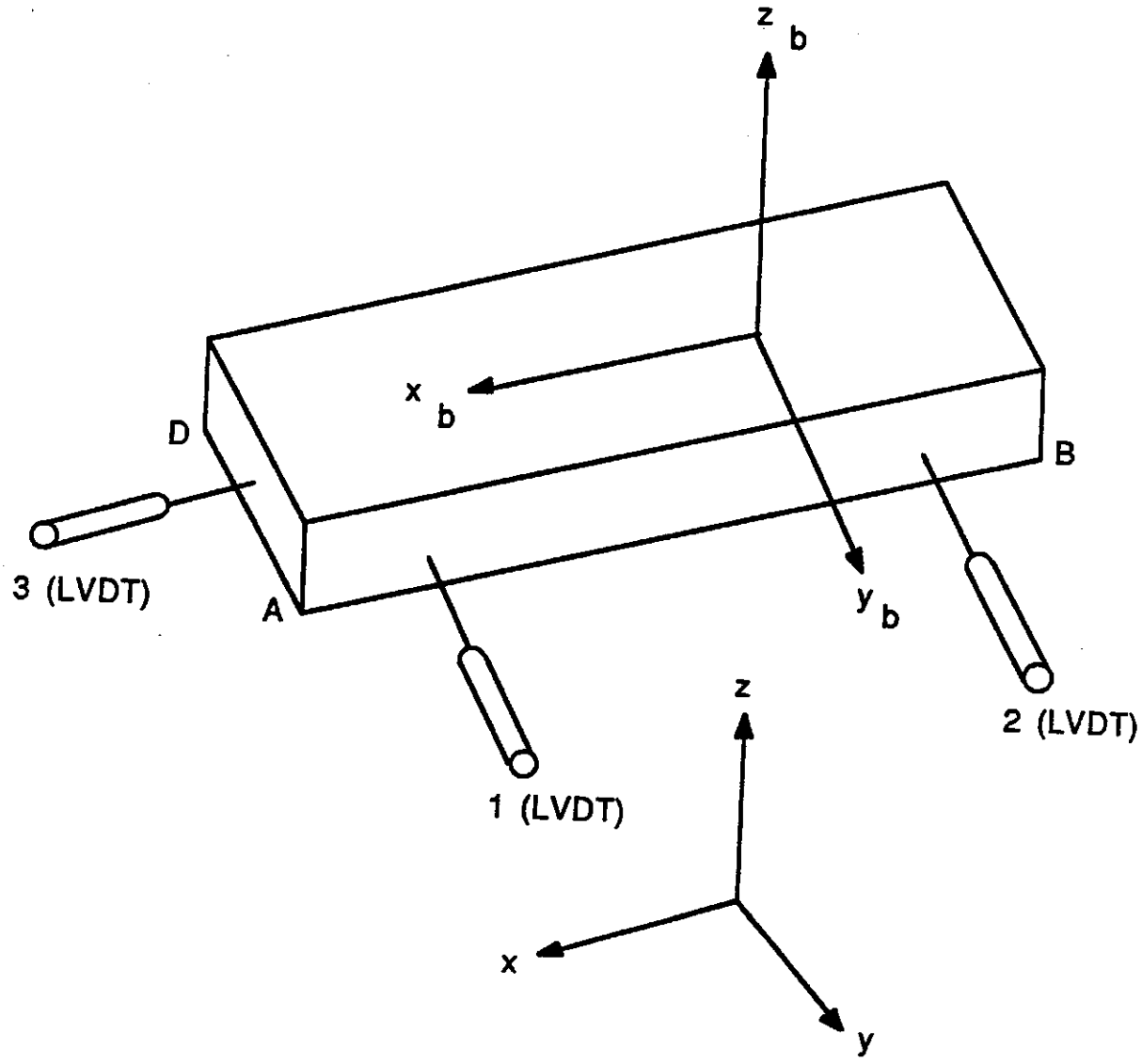

Figure IV.1. The steel beam and sensor locations.

The transformation between the absolute coordinate (x , y , z) and the beam coordinate (x_b, y_b, z_b) is given by

$$\begin{bmatrix} x_b \\ y_b \\ z_b \end{bmatrix} = \begin{bmatrix} n_{xx} & n_{xy} & n_{xz} \\ n_{yx} & n_{yy} & n_{yz} \\ n_{zx} & n_{zy} & n_{zz} \end{bmatrix} \begin{bmatrix} x - x_{cb} \\ y - y_{cb} \\ z - z_{cb} \end{bmatrix} \qquad (2)$$

where n_{xx}, ..., n_{zz} are the directional cosines between the two sets of coordinate axes, x y z and x_b y_b z_b.

The coordinates (x_b, y_b, z_b) of the contact point between the sensor probe and the beam surface must satisfy eq (1), i.e.

$$\begin{bmatrix} a_b & b_b & c_b \end{bmatrix} \begin{bmatrix} x_b \\ y_b \\ z_b \end{bmatrix} = d_b. \qquad (3)$$

Considering only small amplitude oscillations of the lower crane platform it was assumed that the motion of the beam can be approximated by a translation on a horizontal plane and a rotation about a vertical axis. LVDT sensor 1 and 2 were in contact with surface AB of the beam and could measure its angular displacement. Sensor 3 was in contact with surface AD of the beam and in conjunction with sensors 1 and 2 can measure its translation.

Determination of the Beam Angular Displacement

Let the normals to surfaces AB and AD with respect to the beam coordinate frame be (a_1, b_1, 0) and (a_3, b_3, 0), respectively. The unit vector (n_x^b, n_y^b, 0) of the line segment connecting the contact points between sensor probes 1, 2 and surface AB, with respect to the beam coordinate frame, is perpendicular to the surface normal (a_1, b_1, 0). Therefore,

$$(n_x^b, n_y^b, 0) = (-b_1, a_1, 0). \qquad (4)$$

As the beam with the payload moves, its motion can be described by rotation matrices and translation vectors. At any time, the unit vector of the line connecting sensor probes 1 and 2, with respect to the reference coordinate frame, can be represented by

$$\begin{bmatrix} n_x \\ n_y \\ 0 \end{bmatrix} = \begin{bmatrix} \cos\theta_1 & \sin\theta_1 & 0 \\ -\sin\theta_1 & \cos\theta_1 & 0 \\ 0 & 0 & 1 \end{bmatrix} \begin{bmatrix} n_x{}^b \\ n_y{}^b \\ 0 \end{bmatrix} \tag{5}$$

Where θ_1 is the angular displacement of the beam for a rotation about the vertical axis. Provided that sensor probes 1 and 2 always maintain contact with surface AB the unit vector $(n_x, n_y, 0)$ is directly related to the positions measured by the sensor probes 1 and 2. The relations are given by

$$n_x = \frac{x_2 - x_1}{\sqrt{(x_2 - x_1)^2 + (y_2 - y_1)^2}} \tag{6.a}$$

$$n_y = \frac{y_2 - y_1}{\sqrt{(x_2 - x_1)^2 + (y_2 - y_1)^2}} \tag{6.b}$$

From eqs (4) and (5),

$$\begin{bmatrix} -b_1 & a_1 \\ a_1 & b_1 \end{bmatrix} \begin{bmatrix} \cos\theta_1 \\ \sin\theta_1 \end{bmatrix} = \begin{bmatrix} n_x \\ n_y \end{bmatrix}. \tag{7}$$

Therefore, the angle of the beam rotation can be obtained directly by solving eq (7).

$$\begin{cases} \cos\theta_1 = \dfrac{-b_1 n_x + a_1 n_y}{(a_1{}^2 + b_1{}^2)} \\ \sin\theta_1 = \dfrac{-b_1 n_y - a_1 n_x}{(a_1{}^2 + b_1{}^2)} \end{cases} \tag{8}$$

Determination of the Beam Translation

Let (x^b, y^b) be the coordinates of a point located on the beam, with respect to the beam coordinate frame. The coordinates of that same point with respect to the reference coordinate frame are given by

$$\begin{bmatrix} x \\ y \end{bmatrix} = \begin{bmatrix} \cos\theta_1 & \sin\theta_1 \\ -\sin\theta_1 & \cos\theta_1 \end{bmatrix} \begin{bmatrix} x^b \\ y^b \end{bmatrix} + \begin{bmatrix} u_1 \\ v_1 \end{bmatrix} \qquad (9)$$

Where θ_1 represents the angular displacement of the beam coordinate frame with respect to the reference coordinate frame, and (u_1, v_1) the vector of translation between the same frames.

To determine (u_1, v_1), the eqs representing the surfaces to which the sensor probes are in contact must be used. Again, assuming a two-dimensional motion case, the relevant surfaces are represented by

$$\text{Surface AB:} \quad a_1 x_{12}^b + b_1 y_{12}^b = d_1 \qquad (10.a)$$

$$\text{Surface AD:} \quad a_3 x_3^b + b_3 y_3^b = d_3 \qquad (10.b)$$

Where (x_{12}^b, y_{12}^b) is a beam point located on surface AB and (x_3^b, y_3^b) is a beam point located on surface AD. Substituting eq (9) into eqs (10.a) and (10.b), gives

$$a_1 [(x_{12} - u_1) \cos\theta_1 - (y_{12} - v_1) \sin\theta_1] + b_1 [(x_{12} - u_1) \sin\theta_1 + (y_{12} - v_1) \cos\theta_1] = d_1 \qquad (11.a)$$

$$a_3 [(x_3 - u_1) \cos\theta_1 - (y_3 - v_1) \sin\theta_1] + b_3 [(x_3 - u_1) \sin\theta_1 + (y_3 - v_1) \cos\theta_1] = d_3 \qquad (11.b)$$

Where (x_{12}, y_{12}) are the coordinates of a point located on surface AB with respect to the reference frame and (x_3, y_3) are the coordinates of a point located on surface AD with respect to the reference frame.

After rearranging terms, eqs (11a and b) become

$$(a_1 \cos\theta_1 + b_1 \sin\theta_1)\, u_1 + (-a_1 \sin\theta_1 + b_1 \cos\theta_1)\, v_1 = (a_1 \cos\theta_1 + b_1 \sin\theta_1)\, x_{12} + (-a_1 \sin\theta_1 + b_1 \cos\theta_1)\, y_{12} + d_1 \qquad (12.a)$$

$$(a_3 \cos\theta_1 + b_3 \sin\theta_1)\, u_1 + (-a_3 \sin\theta_1 + b_3 \cos\theta_1)\, v_1 = (a_3 \cos\theta_1 + b_3 \sin\theta_1)\, x_3 + (-a_3 \sin\theta_1 + b_3 \cos\theta_1)\, y_3 + d_3 . \qquad (12.b)$$

The sensor readings must satisfy eqs (12a and b).

Let $(x_1, y_1, 0)$, $(x_2, y_2, 0)$, $(x_3, y_3, 0)$, be the sensor readings of probe 1, 2, 3, respectively. Then

$$\begin{aligned} \xi_1 u_1 + \eta_1 v_1 &= \delta_1 \\ \xi_2 u_1 + \eta_2 v_1 &= \delta_2 \\ \xi_3 u_1 + \eta_3 v_1 &= \delta_3 \end{aligned} \qquad (13)$$

where

$$\begin{aligned} \xi_2 = \xi_1 &= a_1 \cos\theta_1 + b_1 \sin\theta_1 \\ \eta_2 = \eta_1 &= -a_1 \sin\theta_1 + b_1 \cos\theta_1 \\ \xi_3 &= a_3 \cos\theta_1 + b_1 \cos\theta_1 \\ \eta_3 &= -a_3 \sin\theta_1 + b_3 \cos\theta_1 \\ \delta_1 &= \xi_1 x_1 + \eta_1 y_1 + d_1 \\ \delta_2 &= \xi_2 x_2 + \eta_2 y_2 + d_2 \\ \delta_3 &= \xi_3 x_3 + \eta_3 y_3 + d_3 \end{aligned}$$

Rewriting eq (13), gives

$$\begin{bmatrix} \xi_1 & \eta_1 \\ \xi_2 & \eta_2 \\ \xi_3 & \eta_3 \end{bmatrix} \begin{bmatrix} u_1 \\ v_1 \end{bmatrix} = \begin{bmatrix} \delta_1 \\ \delta_2 \\ \delta_3 \end{bmatrix} \qquad (14)$$

Multiplying both sides of eq (14) by the transpose of the coefficient matrix, gives

$$\begin{bmatrix} p_1 & q_1 \\ q_1 & r_1 \end{bmatrix} \begin{bmatrix} u_1 \\ v_1 \end{bmatrix} = \begin{bmatrix} \alpha_1 \\ \beta_1 \end{bmatrix} \tag{15}$$

where

$$\begin{aligned} p_1 &= \xi_1^2 + \xi_2^2 + \xi_3^2 \\ q_1 &= \xi_1 \eta_1 + \xi_2 \eta_2 + \xi_3 \eta_3 \\ r_1 &= \eta_1^2 + \eta_2^2 + \eta_3^2 \\ \alpha_1 &= \xi_1 \delta_1 + \xi_2 \delta_2 + \xi_3 \delta_3 \\ \beta_1 &= \eta_1 \delta_1 + \eta_2 \delta_2 + \eta_3 \delta_3 \end{aligned}$$

Solving eq (15), gives the translation vector of the beam as

$$u_1 = \frac{\alpha_1 r_1 - \beta_1 q_1}{p_1 r_1 - q_1^2} \qquad v_1 = - \frac{p_1 \beta_1 - q_1 \alpha_1}{p_1 r_1 - q_1^2}. \tag{16}$$

IV.2 The Control Algorithms

Let the coordinates of an arbitrary point on the beam be (x^b, y^b), with respect to the beam coordinate frame. Equation (9) gives the coordinates (x , y) of the same point with respect to the reference frame. If a target position (x^t, y^t) is specified, the displacement vector required for the point to reach the target position from its current position is

$$\Delta x = x^t - x \qquad \Delta y = y^t - y \quad .$$

The displacement vector (Δx, Δy) is related to the beam increments of the angle of rotation and the translation as follows:

$$\begin{bmatrix} \Delta x \\ \Delta y \end{bmatrix} = \Delta\theta_1 \begin{bmatrix} -\sin\theta_1 & \cos\theta_1 \\ -\cos\theta_1 & -\sin\theta_1 \end{bmatrix} \begin{bmatrix} x^b \\ y^b \end{bmatrix} + \begin{bmatrix} \Delta u_1 \\ \Delta v_1 \end{bmatrix} \tag{17}$$

Defining

$$x^* = -x^b \sin\theta_1 + y^b \cos\theta_1$$
$$y^* = -x^b \cos\theta_1 - y^b \sin\theta_1$$

eq (17) can be rewritten as

$$\Delta u_1 + (\Delta\theta_1)\, x^* = \Delta x \tag{18}$$
$$\Delta v_1 + (\Delta\theta_1)\, y^* = \Delta y \tag{19}$$

Another eq needed to solve for $\Delta\theta_1$, Δu_1 and Δv_1 is obtained by minimizing the following quadratic functional

$$I = \alpha (\Delta u_1)^2 + \beta (\Delta v_1)^2 + \gamma (\Delta\theta_1)^2 \tag{20}$$

resulting in

$$\alpha \Delta u_1 + \beta \Delta v_1 + \gamma \Delta\theta_1 = 0 \tag{21}$$

where α, β, γ are constants. Therefore, the required amounts of beam displacement are obtained by solving eqs (18), (19) and (21):

$$\begin{bmatrix} \Delta u_1 \\ \Delta v_1 \\ \Delta\theta_1 \end{bmatrix} = \begin{bmatrix} 1 & 0 & x^* \\ 0 & 1 & y^* \\ \alpha & \beta & \gamma \end{bmatrix}^{-1} \begin{bmatrix} \Delta x \\ \Delta y \\ 0 \end{bmatrix} \tag{22}$$

An IBM-AT/PC computer was programmed to solve eq (22). The program was written in C language. The feedback signals came from the three LVDT position sensors. Their outputs were filtered by antialiasing filters and then passed through voltage amplifiers to adjust their voltage range (see fig.12). The signals were then digitized by an A/D data acquisition system which was connected and controlled by the computer. At the end of each control cycle the digital command signals were sent to a D/A converter, which was connected and controlled by the computer. The D/A output signals were passed through voltage amplifiers to adjust their range before reaching the three servo-amplifier controllers responsible for driving the three torque motors.

Several square pulse excitation tests were conducted to tune the servo amplifiers and the digital controller. The rise and fall times of the x-y table servo joints for a square pulse amplitude which was 40% of the maximum command signal amplitude were approximately 0.8 seconds. The corresponding times for a square pulse amplitude which was 100% of the maximum command signal amplitude for the rotary joint was 2.5 seconds.